



RESEARCH ARTICLE

10.1002/2016GC006623

Special Section:

Subduction Processes in
Central America With an
Emphasis on CRISP Results

Key Points:

- Statistical analyses used to interpret paleoceanographic changes through time
- Radiolarians as a proxy for paleoceanographic interpretations
- Paleoceanographic events in the eastern equatorial Pacific since late Miocene

Supporting Information:

- Supporting Information S1
- Figure S1
- Figure S2
- Figure S3
- Figure S4
- Figure S5
- Table S1
- Table S2
- Table S3
- Table S4

Correspondence to:

M. I. Sandoval,
mariaisabel.sandoval@ucr.ac.cr

Citation:

Sandoval, M. I., D. Boltovskoy,
A. T. Baxter, and P. O. Baumgartner
(2017), Neogene paleoceanography of
the eastern equatorial Pacific based on
the radiolarian record of IODP drill
sites off Costa Rica, *Geochem. Geophys.
Geosyst.*, 18, doi:10.1002/
2016GC006623.

Received 2 SEP 2016

Accepted 7 FEB 2017

Accepted article online 11 FEB 2017

© 2017. American Geophysical Union.
All Rights Reserved.Neogene paleoceanography of the eastern equatorial Pacific
based on the radiolarian record of IODP drill sites off Costa RicaMaría I. Sandoval^{1,2}, Demetrio Boltovskoy³, Alan T. Baxter^{4,5} , and Peter O. Baumgartner¹

¹Institut des Sciences de la Terre, Université de Lausanne, Lausanne, Switzerland, ²Now at Universidad de Costa Rica, Escuela Centroamericana de Geología, San José, Costa Rica, ³Instituto de Ecología, Genética y Evolución de Buenos Aires, Universidad de Buenos Aires-CONICET, Buenos Aires, Argentina, ⁴School of Environmental and Rural Science, University of New England, Armidale, New South Wales, Australia, ⁵Department of Earth and Planetary Sciences, McGill University, Montreal, Quebec, Canada

Abstract The Integrated Ocean Drilling Program (IODP) Expedition 344 drilled cores following a transect across the convergent margin off Costa Rica. Two of the five sites (U1381 and U1414) are the subject of the present study. Major radiolarian faunal breaks and characteristic species groups were defined with the aid of cluster analysis, nodal analysis, and discriminant analysis of principal components. A middle-late Miocene to Pleistocene age (radiolarian zones RN5 to RN16) was determined for the sites, which agrees with the nanofossil zonations and ⁴⁰Ar/³⁹Ar and tephra layers. Considering the northward movement of the Cocos plate (~7.3 cm/yr), and a paleolatitude calculator, it is assumed that during the Miocene the two sites were located ~1000 km to the southwest of their current position, slightly south of the equator. The radiolarian faunas retrieved were thus seemingly formed under the influence of different oceanic currents and sources of nutrients. Changes in the radiolarian assemblages at Site U1414 point at dissimilar environmental settings associated with the colder South Equatorial Current and the warmer Equatorial Countercurrent, as well as to coastal upwelling. These differences are best reflected by changes in the abundance of the morphotype *Spongurus* spp., with noticeably higher values during the Miocene, than in the Pliocene and the Pleistocene. Because *Spongurus* spp. is generally associated with cooler waters, these abundance variations (as well as those of several other species) suggest that during the Miocene the area had a stronger influence of colder waters than during younger periods. During the Pliocene and the lowermost Pleistocene, biogenic remains are scarce, presumably due to the terrigenous input, which could have diluted and affected the preservation of pelagic fossils, as well as to the displacement of the site to warmer waters. A typically tropical fauna characterized the Pleistocene, yet with widespread presence of colder water species, most probably indicative of the influence of coastal upwelling processes.

1. Introduction

From the Miocene to the Recent, the sedimentary record of the Equatorial Pacific Ocean contains abundant and well-preserved radiolarians. Multiple studies, chiefly based on ocean drilling material, have considerably improved the quality of the microfossil data, facilitating the use of radiolarians as a major tool for dating Neogene marine deposits [Riedel and Sanfilippo, 1970, 1978; Johnson *et al.*, 1989; Moore, 1995; Sanfilippo and Nigrini, 1998]. On the other hand, surveys of the geographic and bathymetric distribution of radiolarian species based on water-column samples, including plankton tows [Petrushevskaya, 1971; Renz, 1976; Kling, 1979; Boltovskoy and Riedel, 1987; Kling and Boltovskoy, 1995; Welling, 1997], sediment trap samples [Takahashi, 1991; Boltovskoy *et al.*, 1993, 1996; Okazaki *et al.*, 2003, 2005, 2008], and surface sediment materials [Nigrini, 1967; Renz, 1976; Petrushevskaya, 1971; Morley, 1977; Molina-Cruz, 1977, 1997; Johnson and Nigrini, 1980, 1982; Boltovskoy, 1987; Moore *et al.*, 1980; Pisas *et al.*, 1997; Hollis and Neil, 2005] furnished abundant ecological information which allowed the use of radiolarian fossil assemblages for paleoceanographic reconstructions [see Boltovskoy and Correa, 2016, for a review of the biogeography of Recent Radiolaria]. These works gradually refined our understanding of the association of species-specific radiolarian assemblages with more or less discrete environmental envelopes (chiefly temperature and food availability, as represented by primary production), which in turn are often representative of different water masses, allowing the extrapolation of these relationships to pre-Recent settings.

Studies of microplankton are chiefly based on two sources of material: water-column samples (plankton tows and sediment traps) and sediments samples. Both techniques have their advantages and disadvantages [e.g., *Boltovskoy*, 1994]. The main advantages of sedimentary materials are: (1) A small fraction of the sample is used, the remainder being stored and available for future studies. (2) The sample-size is usually orders of magnitude larger than that needed for any particular micropaleontological survey, whereby only a gram of material can yield tens to millions of microfossils. (3) As opposed to water-column materials, which reflect instantaneous snapshots representative of a very short time-span (days to months), sedimentary samples yield a time-averaged (years or decades to millennia) image of the environmental conditions in the overlying water. On the other hand, disadvantages of sedimentary material include: (1) Fragmentation and dissolution, meaning that only a fraction of the skeletons are preserved in the fossil record, this process being often selective and, occasionally, associated with the area and the thermal envelope of the species. (2) Reworking of the sediments by bioturbation processes of the uppermost strata, bottom currents, and tectonic processes, all of which can alter the original stratification. (3) Winnowing and advection by subsurface and bottom currents can mobilize and displace the shells hundreds and even thousands of kilometers from their living areas in the uppermost water layers, significantly biasing their environmental signal. (4) Differential seasonal dynamics: seasonality is rarely preserved in the fossil record. However, major seasonal shifts in dominant species and differential seasonal production rates can bias the sedimentary assemblages. (5) Species-specific productivity differences, whereby in the sediments, species with high reproduction rates and short-life spans can be overrepresented with respect to those with lower reproductive outputs and longer life spans. (6) Equatorward subsurface transport: because cold-water species expatriated into warmer-water areas can extend their survival by sinking in the water-column in search of lower temperatures, expatriated surface and subsurface planktonic organisms end up dying and sedimenting in areas outside of their home range in the upper layers, thus "contaminating" these deposits with forms that do not normally inhabit the area [e.g., *Boltovskoy and Correa*, 2017]. Despite these shortcomings, radiolarians have proved their usefulness in many paleobiogeographic and paleoecological studies, especially on large-scale time intervals and ample oceanic areas, where the above-described biasing mechanisms are less significant. The present study uses the specific ecological assignments developed in the above mentioned surveys.

In the sediments of the eastern Equatorial Pacific, radiolarians are very diverse and abundant, having been used in several biostratigraphic and paleoceanographic investigations based on DSDP and ODP materials [e.g., *Nigrini*, 1968; *Goll*, 1980; *Haslett*, 1992, 1994, 1995].

According to plate motion vectors (7.3 cm/yr) and the paleolatitude calculator of *van Hinsbergen et al.* [2015], during the late Miocene (~12 Ma), the studied area was located close to the equator (~2°S). Thus, the biogenic remains obtained from the two sites were generated under a range of conditions characterized by different surficial currents and their associated temperatures and primary production values [*Baumgartner*, 2013]. The goal of this work is to identify the influences of both the cold South Equatorial Current and the warm Equatorial Countercurrent, expected to have influenced these sediments. Our results also provide interesting comparative information with reports on radiolarian stratigraphy and paleoceanography in the area [*Molina-Cruz*, 1977, 1997; *Romine*, 1985; *Kamikuri et al.*, 2009a, 2009b].

2. Setting

2.1. Geological Setting

The western active margin off Costa Rica represents the subduction zone resulting from the interaction of the Cocos Plate and the Caribbean Plate. The Cocos Plate is located at the intersection of two ridges: the fast spreading East Pacific Rise (EPR), which currently is the western boundary, and the slow-spreading Cocos Nazca Spreading center (CNS), which currently is the eastern limit [*Harris et al.*, 2013]. The boundary separating the EPR and the CNS crusts is a combination of a triple junction trace and a fracture zone, collectively comprising a "plate suture." The EPR-generated crust has a smoother morphology than the CNS-generated crust [*Harris et al.*, 2013]. The age of the Cocos Plate at the Middle America Trench goes from 24 Ma, offshore the Nicoya Peninsula, to 15 Ma, offshore the Osa Peninsula [southern Costa Rica; *Barckhausen et al.*, 2001]. In the Osa Peninsula, the Cocos Plate is characterized by a rough surface due to the presence of the prominent submarine and aseismic Cocos Ridge (Figure 1), created under the influence of Galapagos hotspot volcanism. The highest peaks reach an elevation of approximately 1000 m below sea level

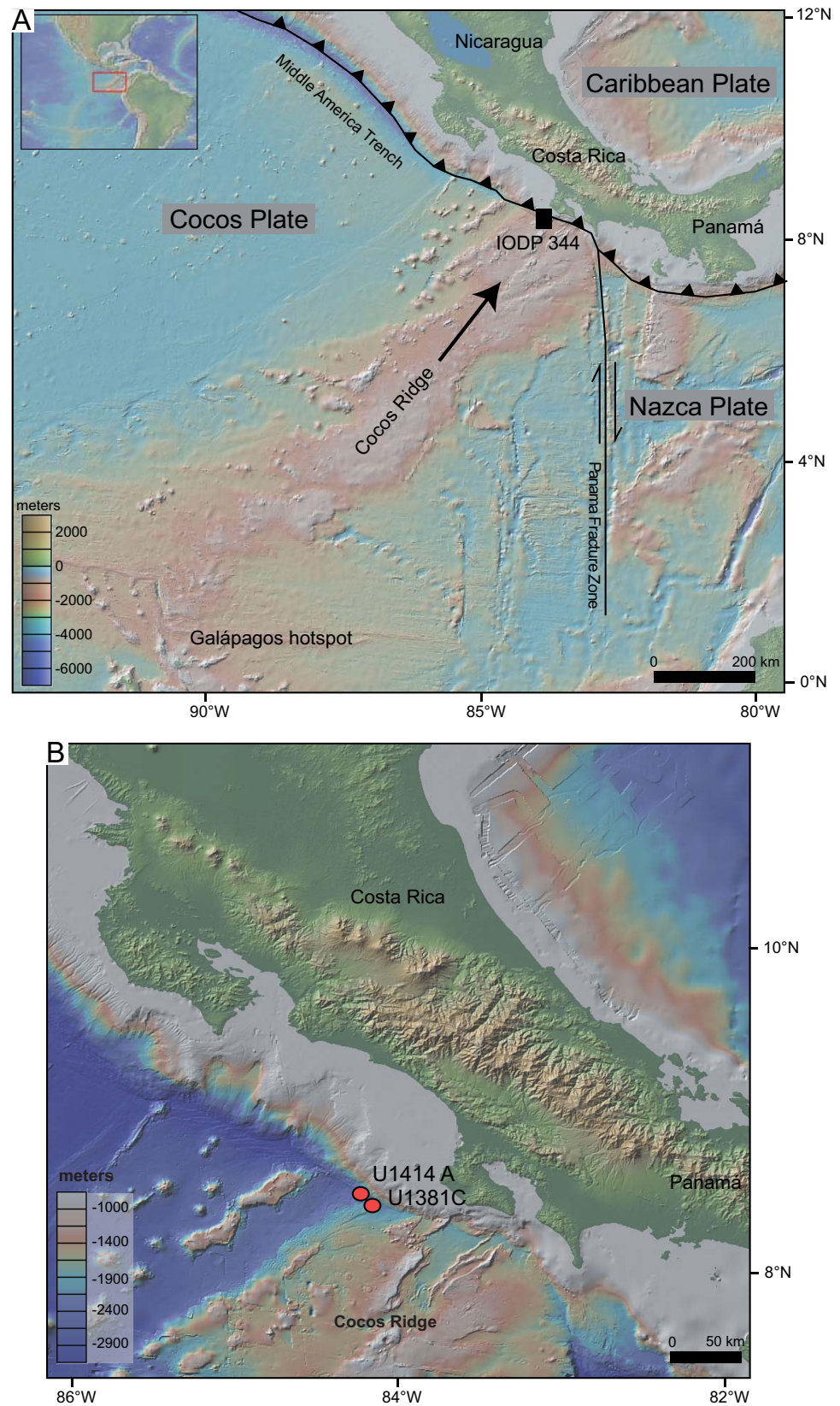


Figure 1. Location of the IODP Expedition 344 in the geological context of western Costa Rica. The topographic map is adapted from www.geomapapp.org [Ryan *et al.*, 2009]. A. General map of western Costa Rica. B. Location of Holes U1414A and U1381C.

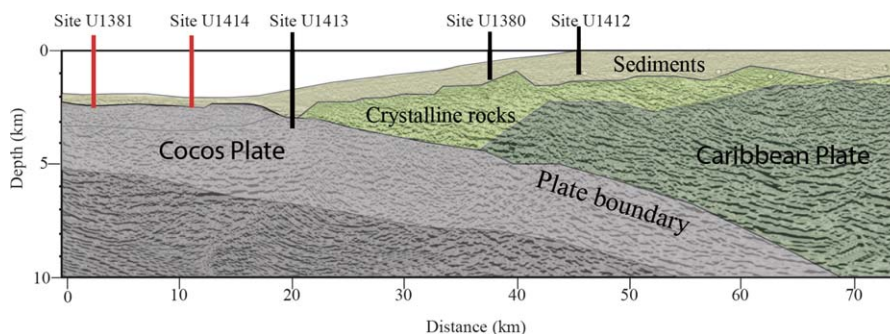


Figure 2. Seismic profile showing the plate boundary in southern Costa Rica. Red marks identify IODP Expedition 344 drilling sites; black marks denote other sites drilled in the area [Stavenhagen *et al.*, 1998; modified after Harris *et al.*, 2013].

[Meschede and Barckhausen, 2000]. These elevations decreased the subduction angle and reduced the depth of the décollement between the two plates. Due to this uneven morphology of the Cocos Ridge, the studied sites are situated along a topographic difference of ~400 m. Site U1414 is located in a flatter and deeper area as compared with Site U1381. The incoming Cocos Plate basement consists of basaltic oceanic crust covered by a relatively thin layer of sediments of approximately 1–2 km (Figure 2).

2.2. Equatorial Pacific Oceanographic Setting

The eastern Equatorial Pacific (~4°N to 20°N, 85°W to 105°W) is the open oceanic region south of Mexico and Central America, and northwest of South America. The region includes the Guatemala Basin and the Cocos Ridge. The area is situated at the crossroads of three major currents: the North Equatorial Current (NEC), the Equatorial Countercurrent (ECC), and the South Equatorial Current (SEC; Figure 3).

The NEC is fed by the California Current (CC), and by water from the eastern Tropical Pacific. In August, its southern boundary lies between approximately 8°N (eastern portion) and 10°N to 12°N (western portion). The NEC stretches between 7°N and 20°N. It carries 20–25 Sv to the west between 10°N and 25°N. Most of this flow is concentrated in the upper 300 m. This current is weak, with speeds below 20 cm/s [Wyrski, 1966].

The ECC flows eastwards between 3°N and 10°N, inside the warm pool region and above 200 m in depth [Yu *et al.*, 2000]. The depth (~10–15 m), speed (~50 cm/s), and transport (~15 Sv) of this current vary seasonally [Stewart, 2008]. The NEC bounds it to the north, while its southern boundary is not always evident. In general, the ECC is closely linked to the Intertropical Convergence Zone (ITCZ), the zone of maximum heating and convergence of the northeast and southeast trade winds. The ECC influences and maintains the Eastern Pacific Warm Pool (EPWP), which is considered the second largest tropical pool in the world.

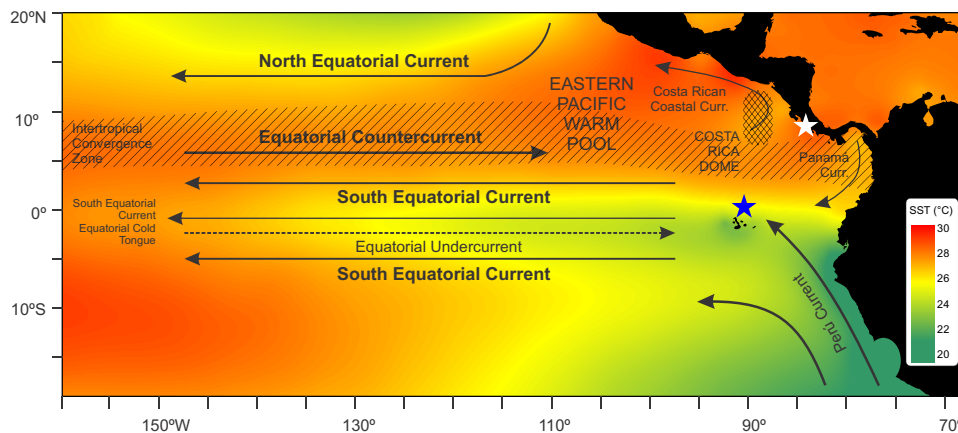


Figure 3. Major oceanographic features and SST (mean for 1995–2012) of the Eastern Tropical Pacific. Blue star: location of the studied sites during late Miocene; white star: recent location. Currents are from Kessler *et al.* [2006] (simplified), mean position of the Intertropical Convergence Zone is from Sachs *et al.* [2009], temperature data are from Boyer *et al.* [2013].

This feature is located offshore of Central America and exhibits constantly warm water ($\sim 27^{\circ}\text{C}$). Interannual changes in the eastward extension of the ECC play a significant role in the formation and development of the El Niño-Southern Oscillation (ENSO) cycles that affect the South American coasts and have worldwide effects [Kamikuri *et al.*, 2009b]. The area east of 90°W is influenced by the Peru Current (PC) and hosts active upwellings and geostrophic divergence.

The South Equatorial Current (SEC), mainly driven by south trade winds, flows to the west between 5°S and 20°S . Its transport reaches 50 Sv, and its velocity can be up to 50 cm/s [Wyrski, 1966]. To the north it is bounded by the ECC.

The Equatorial Undercurrent (EUC), or Cromwell Current, is located beneath the SEC and flows eastward. It is a subsurface current with a maximum velocity of 120 to 150 cm/s at the equator, at about 100 m depth [Wyrski, 1966]. The EUC thickens at the equator, extending approximately between 50 and 200 m depth near the Galapagos Islands. Its transport reaches 34–42 Sv, with temperatures around 13°C . Part of this current flows to the south feeding the PC [Wyrski, 1966].

The Costa Rica Dome (CRD) is located off the Costa Rican coast, between 7°N – 12°N and 88°W – 90°W ; it has a diameter of 200–900 km (Figure 3). The CRD is marked by a relatively shallow (~ 25 m) 20°C isotherm. The dome appears to be the eastern end of the thermocline, which is caused by the reduction of the trade winds. To the east of the CRD, a northwestward flow is known as the Costa Rica Coastal Current (CRCC) [Kessler, 2006]. This current is fed by the stronger branch of the ECC, which splits off upon approaching the coast of Central America [Wyrski, 1966]. The upwelling associated with the CRD produces a nutrient-rich environment.

The Peru Current (PC) flows northwestward along the southern coast of Peru, from 15°S to 5°S [Wyrski, 1966]. It is mainly fed by bottom upwelling water [Molina-Cruz, 1977, 1997].

2.3. Miocene–Pleistocene Oceanographic Context

During the Cenozoic, including the Miocene, the continents and the general circulation pattern and the geographic distribution of gyres and upwelling systems, were similar to those today [Romine, 1985; Lyle *et al.*, 2008], with the exception of the closure of the Central American seaway (CAS). Recent geological and biological studies suggest that the CAS closed at ~ 10 Ma [Brierley and Fedorov, 2016]. This closure gradually precluded the exchange of deep and intermediate water masses along this pathway [Montes *et al.*, 2015; Bacon *et al.*, 2015], but interchange of surface waters was still possible until about 4.7–4.2 Ma [Coates *et al.*, 1992, 2004]. Paleoceanographic models indicate that during the middle Miocene fresh surface waters moved into the Atlantic cooling the surface of this ocean [Krapp and Jungclauss, 2011], but the connection between the surface waters of the Pacific and the Caribbean became restricted at 4.7–4.2 Ma. The inflow of low salinity Pacific waters into the Caribbean was interrupted at 3.5 Ma [Coates *et al.*, 2004], as suggested by the $\delta^{18}\text{O}$ *G. sacculifer* record of the Pacific and the Caribbean [Haug *et al.*, 2001], or even later (~ 2.8 Ma, according to ODea *et al.* [2016]).

The climate during the Cenozoic shows a general global cooling tendency since the onset of Antarctic ice sheet growth at 33.6 Ma [Zachos *et al.*, 2001]. A maximum cooling is reported at 2.5 Ma, with the development of the Northern Hemisphere ice sheets. Superimposed on this general trend, changes between warm and cool periods are recognized.

In the Neogene, the Miocene was marked by two different periods: a warm period, from the early to the middle Miocene (~ 23 – 15 Ma), characterized by a reduced extent of the Antarctic icecap [Zachos *et al.*, 2001] and low CO_2 levels [Pagani *et al.*, 1999]. This warm peak reaches a maximum at 17–15 Ma (Miocene climatic optimum), and is followed by a gradual cooling from the middle to the late Miocene, which is associated with the permanent development of the Antarctic ice sheet [Lyle *et al.*, 2008]. During the late Miocene several important events are recognized, such as the “carbonate crash” (~ 12 – 9 Ma) and the “biogenic bloom” (~ 9 – 4 Ma) [Farrell *et al.*, 1995; Lyle *et al.*, 1995].

In the Pliocene, the climate was generally warm. Several authors suggested permanent El Niño-like conditions during the warm early Pliocene (~ 4.5 – 3 Ma), [Molnar and Cane, 2002; Ravelo *et al.*, 2004, 2006; Wara *et al.*, 2005; Fedorov *et al.*, 2006]. This implies that east-west asymmetry in tropical Pacific Ocean sea surface temperature (SST) and thermocline depth were reduced as compared with present-day values [Ravelo *et al.*, 2006]. SST were $\sim 3^{\circ}\text{C}$ higher than today [Ravelo *et al.*, 2004]. Presently, the tropical Pacific is characterized

by a marked east-west asymmetry. The eastern side has a shallow thermocline (~50 m), and the SST is comparatively cool, while in the west the thermocline is deeper (~200 m), and SST is about 5°C higher. During El Niño events, easterly winds are weaker, which in turn increases eastward water transport by the ECC leading to a more symmetrical pattern of the SST and thermocline depth across the tropical Pacific [Ravelo *et al.*, 2006]. The hypothesis of the El Niño-like Pliocene, however, has been contested by several studies using various paleoclimatic proxies [Rickaby and Halloran, 2005; Watanabe *et al.*, 2011; Zhang *et al.*, 2014]. These contradictions can stem from dissimilar resolution levels, different age-calibration methods, diagenetic overprinting and seawater chemistry changes [Zhang *et al.*, 2014]. The use of radiolarians as a paleoceanographic tool can add to the clarification of these disagreements and the extent of El Niño-like conditions during this period. Modern analogs [e.g., Pisias *et al.*, 1986], pinpointed several western Pacific radiolarians in the eastern Pacific during ENSO events that can be of great value for shedding light on this issue.

3. Materials and Methods

3.1. Sample Preparation

Samples were obtained from two drilling sites of the IODP Expedition 344: Costa Rica Seismogenic Project (CRISP II, Figure 2). The first Site (U1381) is located about 4.5 km seaward of the accretionary prism, offshore Osa Peninsula, on the incoming Cocos plate (8°25.70'N, 84°9.48'W, 2064 m water depth). The core is 109 meters long, and is mainly composed of sediments. The second Site (U1414), also located on the incoming Cocos plate, about 1 km seaward of the deformation front (8°30.23'N, 84°13.53'W, 2459 m water depth), yielded 471.6 m of sediments and basaltic rocks.

The two cores contain calcareous nannofossil-rich ooze with foraminifera, diatoms and radiolarians. Two hundred and ninety-five samples were prepared (69 from Hole U1381C and 226 from Hole U1414A) using standard methods for Neogene sediments [De Wever *et al.*, 2001]. (1) Sediment (10–20 g) was placed in beakers with 100–150 mL of 10% hydrogen peroxide. (2) Samples were boiled for a few minutes to achieve oxidation of the organic matter and disaggregation of the clay fraction. (3) Samples were rinsed with water and sieved through a 60 µm mesh. (4) The wet samples were placed again in beakers adding of a few drops of 10% hydrochloric acid to eliminate foraminifers, nannofossils, and other calcareous remains. (5) The samples were rinsed and sieved again through a 60 µm mesh. (6) A drop of the wet residue (~1 mL) was placed onto a labeled glass slide, dried for a few minutes on a hot plate, embedded in Norland 60 mounting medium, and covered with a coverslip. (7) The slides were exposed for some minutes to ultraviolet light until dry. (8) The mounted samples were analyzed under a transmitted light microscope.

One hundred samples with radiolarians were selected for our analyses (45 from Hole U1381C, and 58 from Hole U1414A). Up to 300 radiolarian individuals per sample were scanned to obtain a representative faunal spectrum [Fatela and Taborda, 2002]. For Hole U1414A, the average was 245 individuals per sample. This site yielded a total of 105 species and 65 taxa with conditional identifications (see supporting information for details, Table S1). For Hole U1381C, the average was 228 individuals per sample, yielding a total of 90 species and 55 taxa with conditional identifications (supporting information Table S2).

3.2. Age Model

The age model (Figure 4) was based on shipboard nannofossil data [Harris *et al.*, 2013], shipboard and post-cruise radiolarian data [Harris *et al.*, 2013; this study], published $^{40}\text{Ar}/^{39}\text{Ar}$ ages of tephra horizons [Schindlbeck *et al.*, 2015, 2016a], and published tephra correlations [Schindlbeck *et al.*, 2016a, 2016b]. In total, 2 nannofossil datums, 2 tephra ages and 15 tephra correlations were used to construct the age model for Hole U1381A; and 4 nannofossil datums, 3 radiolarian datums, 1 tephra age, and 19 tephra correlations for the age model for Hole U1414A. In addition to the first occurrences (FO) and last occurrences (LO) of individual species (supporting information Figures S1–S4), we also defined radiolarian and nannofossil biozones on the basis of shipboard preliminary observations (nannofossils), and both shipboard and post cruise studies (radiolarians). Radiolarian biozones follow the zonation for the tropics proposed by Sanfilippo and Nigrini [1998], whereas nannofossil biozones used the zonation scheme of Martini and Worsley [1970], calibrated to the timescale of Gradstein *et al.* [2012]. The ages of the radiolarian and nannofossil biomarker events used for the age-depth model (Figure 4) were adopted from the program *TS Creator* [Ogg *et al.*, 2016], and from Gradstein *et al.* [2012], respectively.

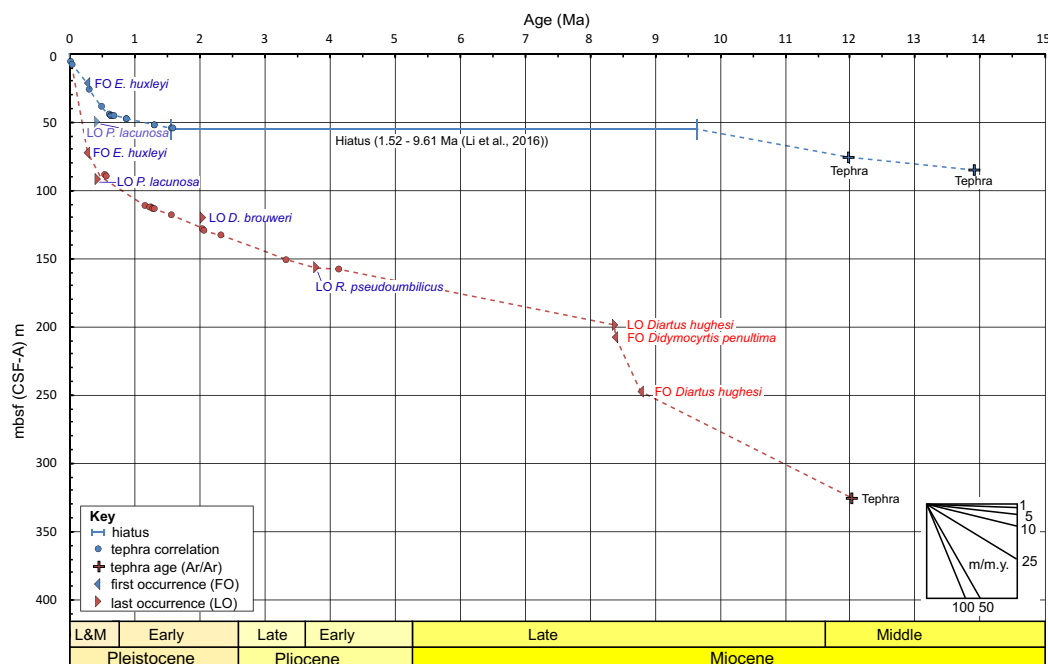


Figure 4. Age model for Site U1414 (red dashed line) and U1381 (blue dashed line) based on shipboard nannofossil and radiolarians datums, ⁴⁰Ar/³⁹Ar tephra ages, and tephra correlations. See also supporting information Tables S3 and S4.

Mean sedimentation rates at Hole U1381C are 54 m/my for the first ~50 m, with a decrease to 10 m/my between 50 m and the Unit I/Unit II boundary (~55 mbsf). Sedimentation rates for the Miocene Unit II (56–100 mbsf) are generally within the range of open-ocean, deep-sea marine sediments (~5 m/my). At Site U1414, sedimentation rates are around 150 m/my for the first 0.5 Ma (~90 mbsf), decreasing steadily throughout the middle Pliocene to ~9.3 m/my (4.15–3.35 Ma; 160 mbsf). Based on the age model, sedimentation rates in this core were highest in the late Miocene (12.05–8.39 Ma, 250–330 mbsf) (~35 m/my).

3.2.1. Radiolarians Constraints

3.2.1.1. Site U1381

Two distinct radiolarian assemblages were observed in Hole U1381C. The upper assemblage (Sections 2H-4W, 66–68 cm to 7H-1, 24–26 cm, 13.36–55.84 mbsf) represents a Pleistocene-Holocene sequence within Unit I. The lack of important radiolarian biostratigraphic species precluded age assignments of this interval. However, the presence of *Amphirhopalum ypsilon* and *Spongaster tetras* from Section 5H-1, 27–31cm, (36.87 mbsf), to the top of the hole suggests a Late Pliocene–Pleistocene age. There is a significant hiatus between

Table 1. Thermal Affinities of Selected Radiolarian Species^a

Species/Group	Ecology	Age	Source
<i>Collosphaera</i> spp.	Warm water		
<i>Heliodiscus asteriscus</i>	Warm water	Miocene-Recent	<i>Nigrini and Lombardi</i> [1984]
<i>Hexapyle</i> spp.	Warm water		
<i>Lamprocyclus maritimalis</i>	Warm water	Miocene-Recent	<i>Nigrini and Lombardi</i> [1984]
<i>Tetrapyle octacantha</i> group	Warm water	Late Miocene-Recent	<i>Nigrini and Lombardi</i> [1984]
<i>Zygocircus productus</i> group	Warm water	Miocene-Recent	<i>Nigrini and Lombardi</i> [1984]
<i>Actinomma langii</i>	Cold water		
<i>Botryostrobus aquilonaris</i>	Cold water	Late Miocene-Recent	<i>Nigrini and Lombardi</i> [1984]
<i>Cornutella profunda</i>	Cold water	Miocene-Recent	<i>Nigrini and Lombardi</i> [1984]
<i>Cycladophora davisiana</i>	Cold water	Miocene-Recent	<i>Moore et al.</i> [1993]
<i>Dictyophimus infabricatus</i>	Cold water	Miocene-Recent	
<i>Pterocorys minythorax</i>	Cold water	Miocene-Recent	<i>Haslett</i> [2003]
<i>Spongurus</i> spp.	Cold water	Miocene-Recent	<i>Nigrini and Lombardi</i> [1985]
<i>Spongopyle osculosa</i>	Cold water	Miocene-Recent	<i>Nigrini and Lombardi</i> [1984]

^aBased on *Molina-Cruz* [1977, 1997], *Kling* [1979], *Kling and Boltovskoy* [1995], and *Kamikuri et al.* [2009b]. Age assignments are based on the references detailed in the body of the table.

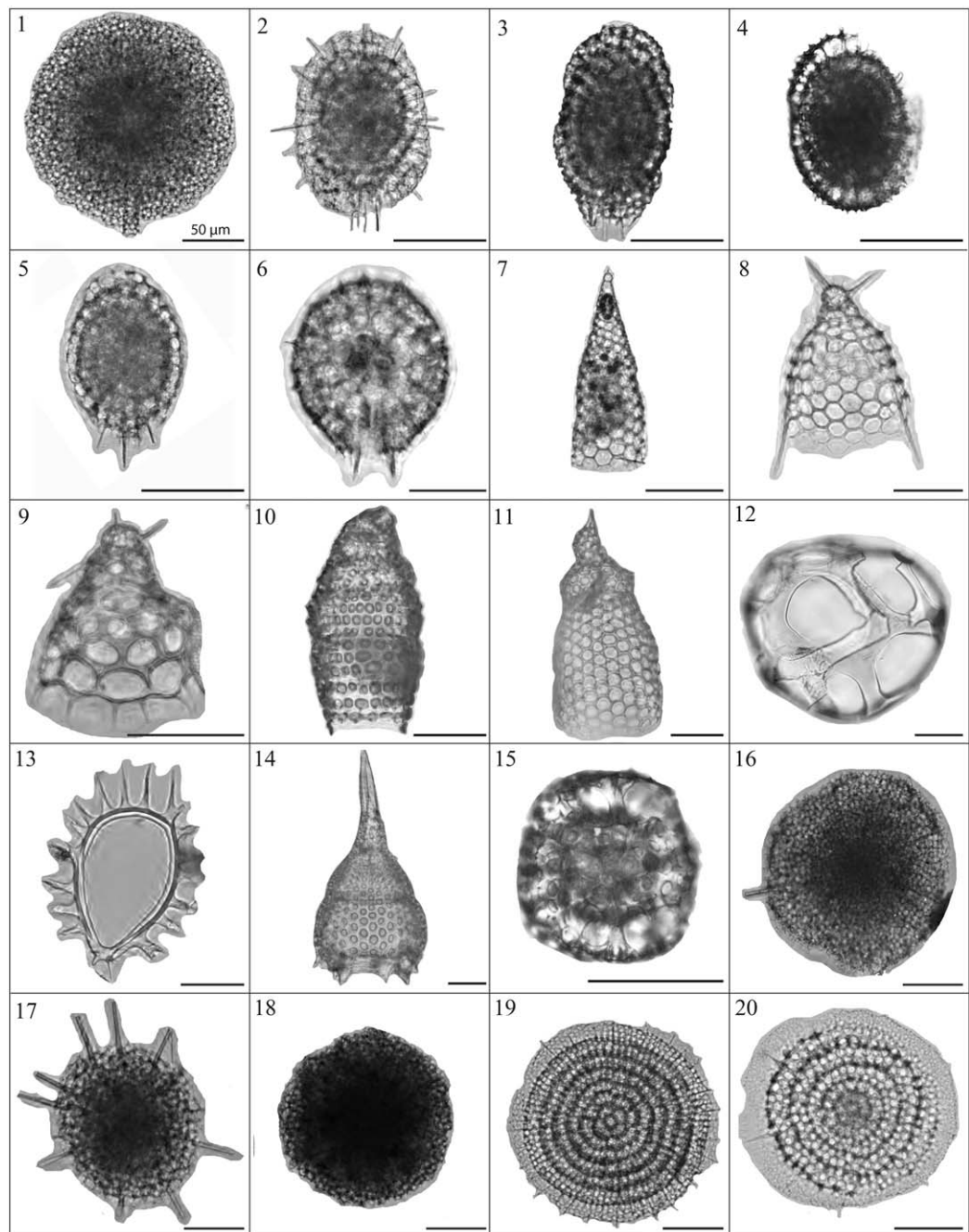


Figure 5. (1–10) Cold-water species. (1) *Spongopyle osculosa* Dreyer (U1414A 1H 1W, 24–26 cm, Pleistocene); (2–5) *Spongurus* spp. (U1414A 1H 1W, 2–4 cm, Pleistocene; U1414A 23X 6W, 24–26 cm, late Miocene); (6) *Actinomma langii* (Dreyer) (U1414A 2H 5W, 17–22 cm, Pleistocene); (7) *Cornutella profunda* Ehrenberg (U1414A 2W 5W, 17–22 cm, Pleistocene); (8) *Dictyophimus infabricatus* Nigrini, (U1414A 1H 1W, 2–4 cm Pleistocene); (9) *Cycladophora davisiana* Ehrenberg (U1414A 1H 1W, 24–26 cm, Pleistocene); (10–20) Warm water species. (10) *Botryostrobus aquilonaris* (Bailey) (U1414A 1H 1W, 24–26 cm, Pleistocene); (11) *Pterocorys minythora* (Nigrini) (U1414A 1H 1W, 24–26 cm, Pleistocene); (12) *Collosphaera macropora* Popofsky (U1414A 28X 7W, 24–26 cm, late Miocene); (13) *Zygocircus productus* group (Hertwig) (U1414A 1H 1W, 2–4 cm, Pleistocene); (14) *Lamprocyclus maritalis* Haeckel (U1414A 11H 3W, 33–35 cm, Pleistocene); (15–20) Cosmopolitan species. (15) *Phortidium pylonium* group Haeckel (U1414A 30X 5W, 22–24 cm, late Miocene); (16–18): (16–17) *Spongotrochus* spp. (U1414A 1H 1W, 2–4 cm, Pleistocene, (18) U1414A 30X 4W, 20–22 cm, Miocene); (19–20) *Stylodictya* spp. (19) U1414A 26X 7W, 16–18 cm, late Miocene; (20) U1414A 30X 5W, 22–24 cm, late Miocene).

Units I and II. The lower assemblage, in Unit II (Sections 7H-1, 37–39 cm to 11H-3, 46–48 cm), (55.97–97.06 mbsf) is characterized by the presence of *Stichocorys armata*, *Didymocyrtis mammifera*, and *Didymocyrtis basanii*, which indicate a middle to late Miocene age (radiolarian biozone RN5) (see supporting information Figures S2 and S3).

3.2.1.2. Site U1414

Hole U1414A contains eight radiolarian zones (supporting information Figures S1 and S3). An interval with few radiolarians is observed in Cores 16H to 21H (~100 m to 200 mbsf), where four biozones appear to be missing. The few specimens observed in this interval did not include any stratigraphically useful indicators. Radiolarian-based correlation between Holes U1381C and U1414A is uncertain. For example, the RN5 zone, recognized in Hole U1381C, is not present in U1414A (compare supporting information Figures S1 and S2).

3.3. Ecological Considerations

Paleoceanographic analyses of Holes U1381C and U1414A are based on the modern ecology of eastern equatorial Pacific radiolarians (Table 1). Species considered as characteristic of deep, intermediate and upwelling water are pooled here in the category of cold-water species (Figure 5).

3.4. Statistical Methods

To interpret the distribution of radiolarians through time, multivariate analyses were carried out. Because many radiolarians were assigned conditional identifications, and some were very scarce or had stratigraphically limited distribution ranges, the database was filtered retaining only the ecologically significant forms and those that ranged throughout all our samples (Table 1, Figure 5; see also supporting information Table S1 and Figure S5). Two different, complementary, approaches were used: (1) A Q-mode cluster analysis [Romersburg, 1984]; program PAST v.2.17 [Hammer et al., 2001], followed by a nodal analysis [Boesch, 1977], performed in Excel v.14.6.6; and (2) A Discriminant Analysis of Principal Components (DAPC) [Jombart et al., 2010], performed in R package adegenet 2.0.0 [Jombart and Collins, 2015].

3.4.1. Q-Mode Cluster Analyses and Nodal Analysis

The cluster analysis of the samples was based on a quantitative (% contribution of each species in the samples) similarity index widely used in ecological studies—the Bray-Curtis index. Clustering was performed with the Unweighted Pair Group with Arithmetic Averages (UPGMA). The sample groups defined by the clusters were then used as units for a Nodal Analysis to identify the species responsible for the classification obtained. Two complementary measures of the affinity of each species for each sample cluster were calculated. Constancy, or the % of the samples in each cluster where the species was recorded; and Fidelity, which is the mean % contribution of the species to each sample group defined by the cluster divided by its mean % contribution to the entire collection [Boesch, 1977]. This approach has been applied previously in radiolarian studies with satisfactory results [Boltovskoy, 1987; Boltovskoy and Riedel, 1987].

3.4.2. Discriminant Analysis of Principal Components (DAPC)

The Discriminant Analysis of Principal Components (DAPC) is a method developed and implemented in the adegenet R packages [Jombart, 2008]. It partitions the samples analyzed into discrete groups based on their specific contents synthesizing the overall variability in a few variables (the discriminant functions). This analysis is closely related to an analysis of variance (ANOVA), but it maximizes the ratio of the variance among groups and minimizes the variance within groups [Montano et al., 2013]. The Bayesian Information Criterion (BIC) is first used to establish the best number of groups comparing the decrease of the residual variance among different numbers of groups, with the best number corresponding to the lowest BIC value [Jombart et al., 2010]. Subsequently, DAPC is performed with the number of clusters indicated by the BIC curve. This analysis comprises a classical Principal Components Analysis, and then the discriminant analysis itself, which is applied to the matrix of principal components. All estimates were performed using the R package adegenet 2.0.0 [Jombart and Collins, 2015].

4. Radiolarian Analysis Through Time, a Tool for Paleocceanographic Interpretations

4.1. Overview of Radiolarian Abundances in Sites U1414 and U1381

At Site U1381, during the middle Miocene the number of morphotypes is relatively constant (Figure 6; see supporting information Table S2 for preservation details and radiolarian counts), decreasing in the vicinity of the hiatus. During the Pleistocene, species richness increases toward the Recent, but is generally lower than in the middle Miocene. Comparison of these figures with those of specific diversity (Shannon-Wiener index [Shannon, 1948]) indicates that during the middle Miocene the diversity was constant and moderate (~2–3). An important drop is observed before the hiatus, followed by a slight increase during the

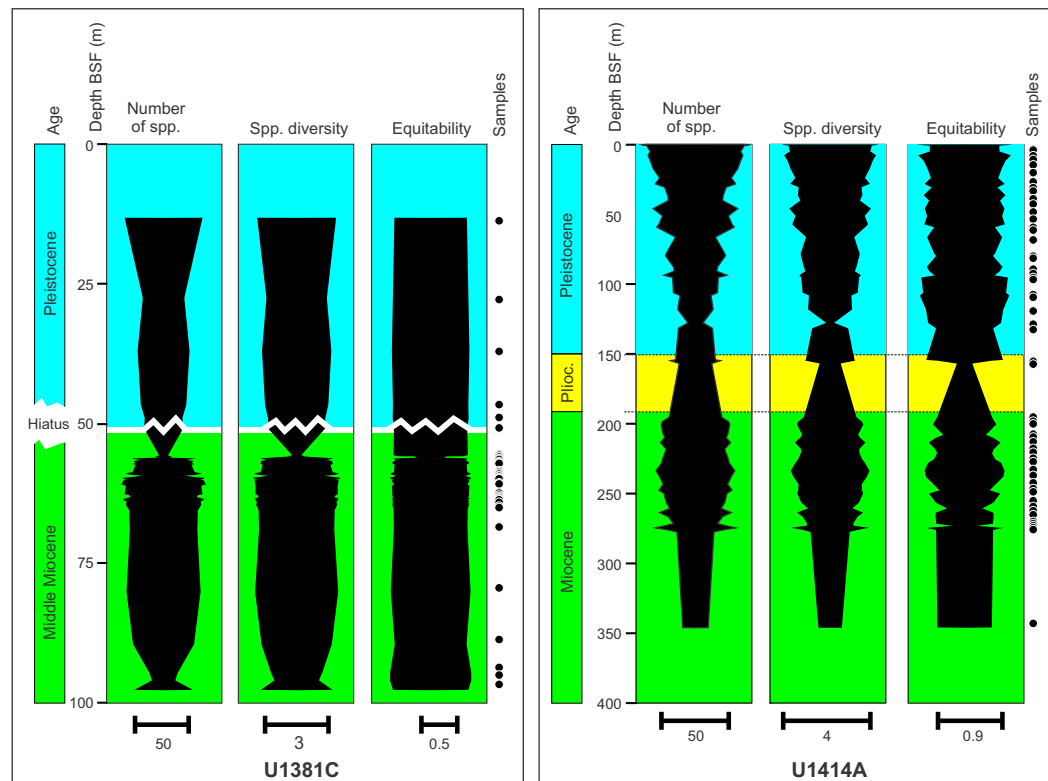


Figure 6. Numbers of species, species diversity (Shannon-Weaver, formula based on Ln), and equitability (Shannon-Weaver diversity divided by the logarithm of the number of taxa—a measure of the evenness of the distribution of individuals between the species), for the two sites investigated

Pleistocene. The Equitability varies little, suggesting that species diversity is chiefly driven by the number of taxa, rather than by changes in their dominance (Figure 5).

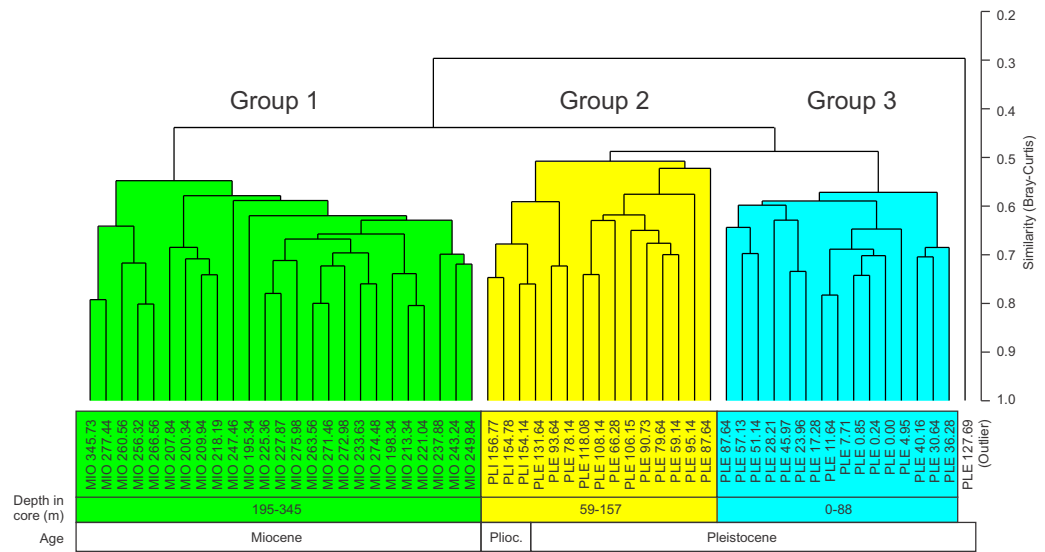
In the lower part of Site U1414 the total number of taxa is scarce, and also the preservation of the samples is poor (Figure 6 and supporting information Table S1). Radiolarian taxa richness increases between ~275 and 200 mbsf (late Miocene) where a conspicuous trough occurs at the end of the Miocene, followed by low numbers in the Pliocene and lowermost Pleistocene, also associated with poor radiolarian preservation. At ~100 mbsf (Pleistocene) the number of species recovers significantly, peaking in the upper section of the core. Diversity and equitability follow a similar pattern, increasing during the late Miocene, dropping in the Pliocene, and again increasing to moderate values (2–3) during the Pleistocene (Figure 6).

4.2. Statistical Analyses

Data from Site U1381 were not used for paleoceanographic analyses due to the presence of a ~8 my hiatus [Li et al., 2016].

Figure 7 illustrates the most conspicuous breaks in faunal similarities recorded at Site U1414. The cluster clearly separates the samples into three chronologically consistent groups. The first group is represented by all the Miocene samples, whereas the two others, more closely interrelated, comprise the three Pliocene and most of the lower Pleistocene samples (group 2), and most of the upper Pleistocene samples (group 3). As mentioned above, the taxa involved (41 species or species groups were selected for our paleoceanographic analyses; see selected data in supporting information Table S1 and Figure S5 for the biostratigraphic distribution of these taxa) are radiolarians present throughout the entire time-span covered, and therefore these results are presumably not biased by evolutionary processes.

Cluster analyses are helpful for grouping faunistically similar samples, but without additional manipulation of the data, they do not furnish information on the species responsible for the groupings obtained. In order to pinpoint the taxa responsible for the groups identified by the cluster, a nodal analysis was performed



	Const.	Fid.	Const.	Fid.	Const.	Fid.
<i>Stylodictya</i> spp.	100.0	1.5	94.1	0.9	86.7	0.4
<i>Spongurus</i> spp.	100.0	1.8	94.1	0.5	100.0	0.3
<i>Larcospira quadrangula</i>	100.0	1.7	41.2	0.4	66.7	0.5
<i>Heliodiscus asteriscus</i>	100.0	1.8	58.8	0.6	33.3	0.2
<i>Stylatractus</i> spp.	65.2	1.6	35.3	0.5	60.0	0.7
<i>Theocorys</i> spp.	34.8	2.2	0.0	0.0	13.3	0.3
<i>Theocorythium</i> spp.	21.7	1.4	5.9	0.5	13.3	0.9
<i>Spongotrochus</i> spp.	100.0	0.9	100.0	1.4	100.0	0.7
<i>Phorticium pylonium</i> group	95.7	0.7	100.0	1.5	100.0	0.9
<i>Stylosphaera</i> spp.	65.2	0.6	82.4	1.7	73.3	0.9
<i>Acrosphaera</i> spp.	52.2	0.7	88.2	1.7	73.3	0.8
<i>Ceratocyrtilis</i> group	26.1	0.6	58.8	1.8	33.3	0.6
<i>Lychnodictyum audax</i>	13.0	0.2	47.1	2.3	20.0	0.8
<i>Actinomma langii</i>	95.7	0.6	94.1	1.2	100.0	1.3
<i>Circodiscus</i> spp.	78.3	0.4	76.5	1.3	100.0	1.5
<i>Anthocyrtilidum</i> spp.	69.6	0.7	41.2	0.6	100.0	1.9
<i>Spongocore</i> spp.	43.5	0.5	41.2	0.9	100.0	1.9
<i>Lophophaena</i> spp.	17.4	0.3	47.1	1.4	86.7	1.6
<i>Euchitonia</i> spp.	34.8	0.8	29.4	0.6	80.0	1.7
<i>Eucyrtidium hexag/acuminatum</i>	8.7	0.1	29.4	0.8	80.0	2.7
<i>Tetrapyle octacantha</i> group	34.8	0.4	47.1	1.4	73.3	1.5
<i>Cycladophora davisiana</i>	26.1	0.5	35.3	0.7	73.3	2.1
<i>Phormostichoartus corbula</i>	17.4	0.2	17.6	0.4	73.3	2.8
<i>Dictyophimus</i> spp.	26.1	0.3	35.3	1.1	66.7	1.8
<i>Dictyophimus infabricatus</i>	8.7	0.3	5.9	0.2	66.7	3.0
<i>Anthocyrtilidum ophirensense</i>	4.3	0.1	5.9	0.2	60.0	3.3
<i>Lampromitra</i> spp.	26.1	0.8	11.8	0.6	46.7	1.7
<i>Lamprocyrtis</i> spp.	26.1	1.2	11.8	0.2	40.0	1.6
<i>Peripyramis circumtexta</i>	26.1	0.7	17.6	1.1	33.3	1.3
<i>Lipmanella dictyoceras</i>	4.3	0.2	5.9	0.3	33.3	3.0
<i>Botryocyrtis</i> spp.	13.0	0.9	0.0	0.0	26.7	2.3
<i>Lamprocyclus maritialis</i>	4.3	0.1	17.6	1.3	26.7	2.1

Figure 7. Cluster analysis (Bray-Curtis similarity, UPGMA, Cophenetic Correlation = 0.750) based on the 41 radiolarians present in both the Miocene and the Pleistocene. Bottom plot shows the results of a nodal analysis of the 32 radiolarians whose highest Constancy (% of the samples in each cluster where the species was recorded), and Fidelity (mean % contribution of the species to each sample group defined by the cluster analysis divided by their mean % contribution to the entire collection) coincided in the same sample group. One sample (PLE 127.632, "outlier" in the cluster) was excluded from the estimates of the nodal analysis. Highest Constancy and Fidelity values for each group of samples are colored.

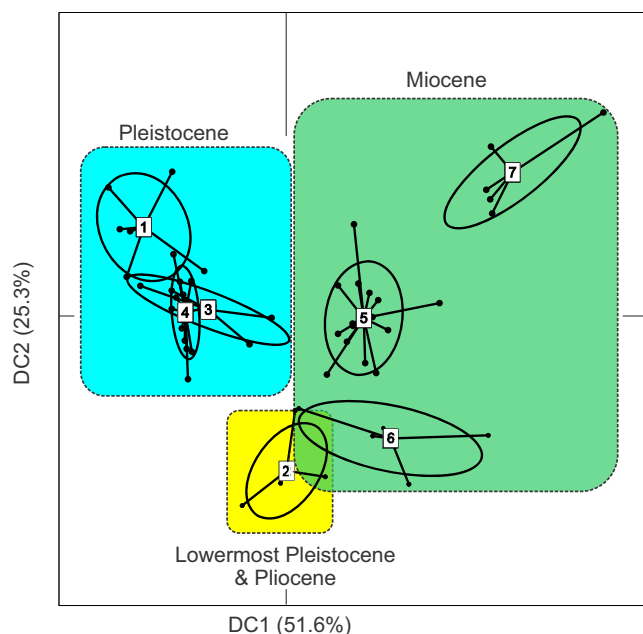


Figure 8. Scatterplot of the samples' coordinates onto the discriminant components 1 and 2. Filled circles denote samples; ellipses are proportional to the internal variance of the groups. Numbers in parentheses along the axes are proportions of total variance accounted for (normalized Eigenvalues). See Figure 9 for loadings of the species on these two axes.

and nodal analyses, a Discriminant Analysis of Principal Components (DAPC) was performed using the same 41 taxa species as those used in cluster/nodal analysis (Figure 8). Cluster/nodal analyses allow a straightforward examination of the significance of each individual taxon, whereas DAPC relies heavily on the principal components, while the significance of species with low abundance values is minimized. In contrast, DAPC allows examining the data under a different perspective, pinpointing the faunal components, which contribute the most to the internal structure of the data.

In DAPC, the BIC indicated that the number of sample groups best accommodated by the data is seven, which was the number of sample groups used in the DAPC. The relative positions of these seven groups, as defined by the discriminant functions, are represented in the scatterplot of Figure 8, generally confirming the faunal differences between Miocene, Pliocene and Pleistocene samples. Discriminant Component 1 (DC1) clearly separated groups 1, 3, and 4 (Pleistocene) from groups 5, 6, 7 (Miocene), whereas group 2 (Pliocene, Pleistocene) was located between the former.

DC2 separated groups 2 and 6 (Pliocene-lowermost Pleistocene and Miocene, respectively) from all the other samples (Figure 8).

Loadings of the taxa on the DCs furnish a measure of their respective importance for the separation of the sample groups defined (Figure 9). *Spongurus* spp., *Stilodictya* spp. are the radiolarians that most strongly contribute to compositional differences in the samples along the x axis (DC1), which accounts for most on the variance (51.6%, see Figure 8). The y axis (DC2) has a much lower Eigenvalue (25.3%), and reflects compositional differences between sample groups 2, 6 and the rest of the collection. *Spongurus* spp. loads heavily on this DC2 as well, but highest values are those of *Spongotrochus* sp. and the family Collosphaeridae (Figure 9).

4.3. Discussion

4.3.1. The Miocene

The late Miocene (biozones RN6 to RN8, Figure 10) is characterized by high abundances and occurrences of *Spongurus* spp. This form is characteristic of cold, deep and/or upwelling waters [Kling and Boltovskoy, 1995]. The dominance of this group suggests that, in the late Miocene, the area was influenced by colder

(Figure 7, lower panel) Samples encompassed by the first cluster (group 1, Miocene) are characterized by particularly higher values of fidelity and constancy of *Spongurus* spp., *Heliodiscus asteriscus*, *Larcospira quadrangula*, *Stylodictya* spp. In group 2 (Pliocene and lowermost Pleistocene), *Spongotrochus* spp. *Phorticium pylonium* group, *Acrosphaera* spp., and *Stylosphaera* spp. were conspicuously more common and abundant than elsewhere. The third group (Pleistocene) was chiefly characterized by *Spongocore* spp., *Anthocyrtidium* spp., *Circodiscus* spp., and *Actinomma langii*. It should be noticed that not all these taxa are readily interpretable in ecological or paleoecological terms, and therefore, in the context of this work, in several cases their use as paleoenvironmental indicators is limited (see Table 1 for a listing of the paleoenvironmentally most important forms).

To validate the results of the cluster

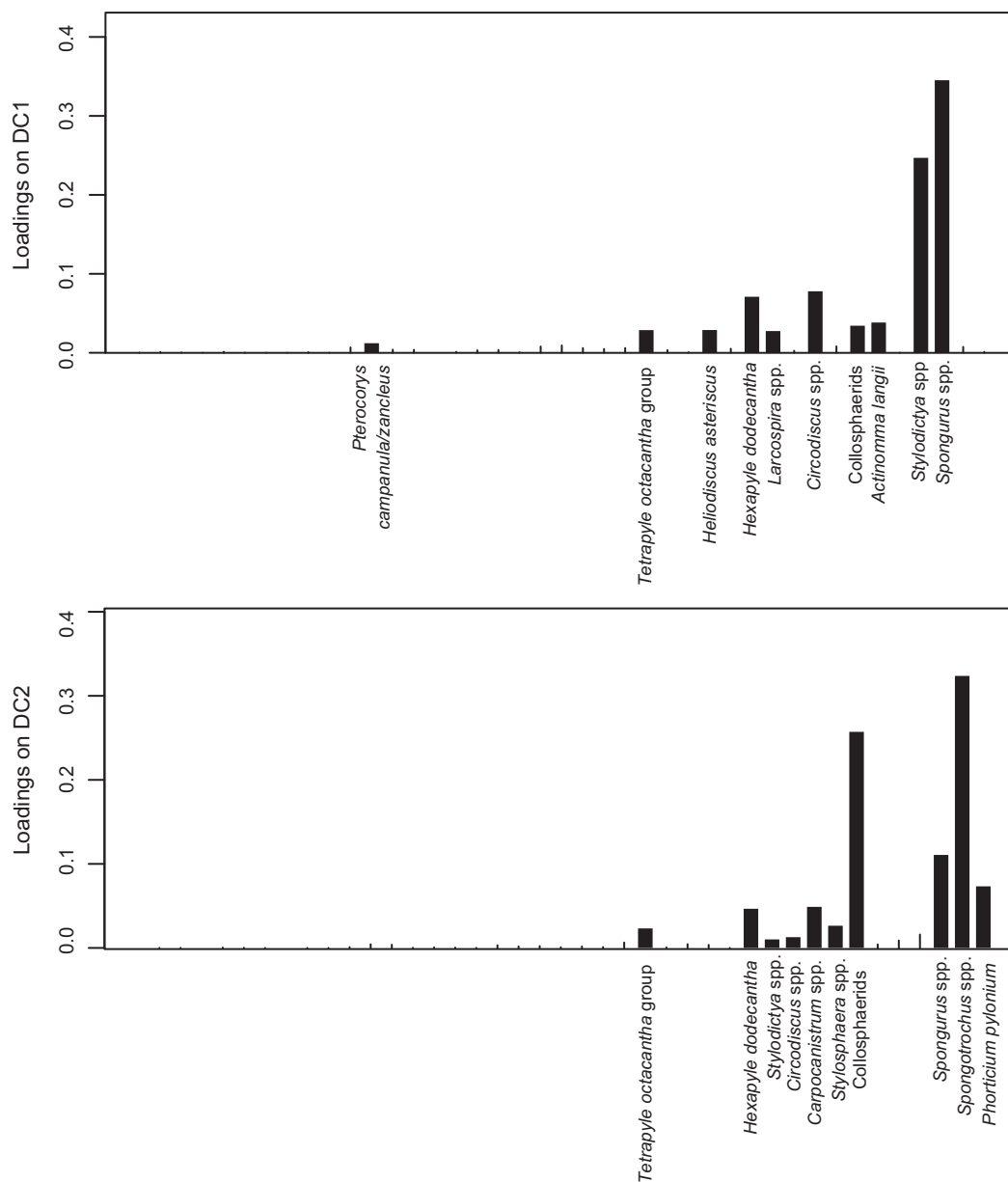


Figure 9. Most significant species loadings on the two discriminant components shown in Figure 8. Notice that *Spongurus* spp. is chiefly responsible for the differences between the Miocene (groups 5–7), the Pliocene–lowermost Pleistocene (group 2), and the Pleistocene (groups 1, 3, 4) (DC1 in Figure 8), whereas the Pliocene–lowermost Pleistocene (group 2) and part of the Miocene (group 6) differ most from all other samples in the loadings of *Spongotrochus* spp. and Collosphaeridae.

waters than today, probably represented by the cold equatorial tongue of the South Equatorial Current and upwelling water associated with the Peru Current (Figure 3). In the Miocene this was located close to the equator, where the influence of these currents is significantly stronger (Figure 3). Further, during this period, the CAS was closing, leading to a general reorganization of circulation patterns in the area. The ~8 my hiatus observed in Hole U1381C could be the result of this reorganization, which in turn affected sedimentation rates. This hiatus is not restricted to the site investigated, but seems to be a regional feature [e.g., Site U1241 of ODP Leg 202 (Cocos Ridge), and in Hole U1381A of IODP Exp. 334 (Cocos Plate); see also Moore *et al.*, 1978]. According to Keller and Barron [1983], these Miocene gaps throughout the eastern equatorial Pacific represent major erosional events related to bottom currents. Other possible causes are tectonic changes associated with the displacement of these sites toward the accretionary prism of the subduction zone [Mix *et al.*, 2003]. Thus, both local tectonics and the large-scale effects of the closure of the CAS may

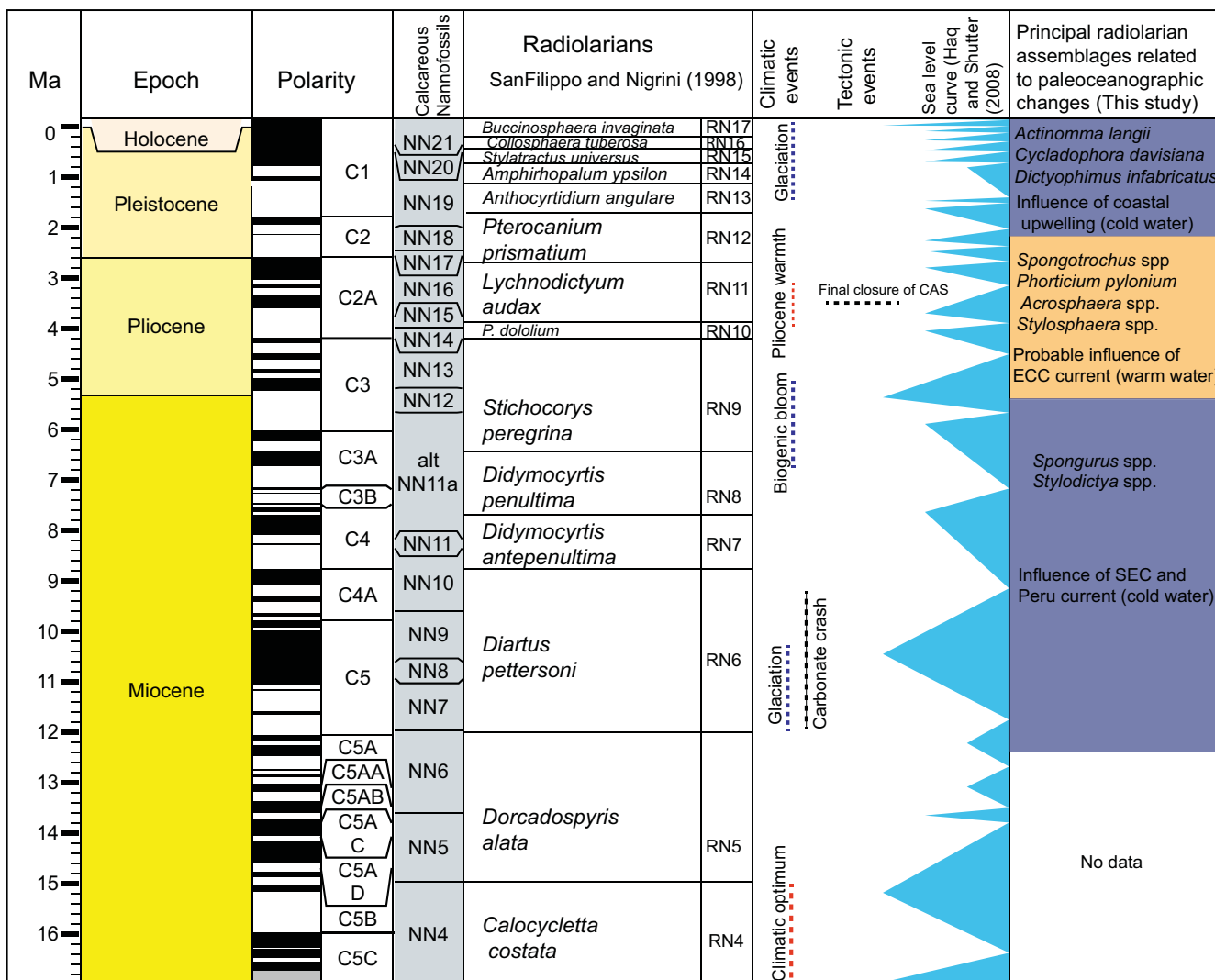


Figure 10. Main radiolarian assemblages and major paleoceanographic changes at Hole U1414 A. Climatic events are based on Zachos et al. [2001], Farrell et al. [1995], and Lyle et al. [1995]. Tectonic events are from Coates et al. [2004]. ECC: Equatorial Countercurrent, SEC: South Equatorial Current (Time Scale Creator program, Version 5.4).

explain the lack of sediment accumulation or the tectonic removal of the missing upper Miocene to Pleistocene sedimentary sequence at Site U1381. However, despite their widespread occurrence, these hiatuses are not a rule in the area, as indicated by the nearby Site U1414, which yielded a complete and well-preserved sedimentary sequence. This contrast may be explained by the fact that Site U1414 is located in a topographically more favorable location, flatter and ~400 m deeper than Site U1381 and several other previously drilled sites. Major hiatuses occur primarily beneath topographic highs, in the path of strong bottom currents [Keller and Barron, 1983]. This topographic effect on sediment accumulation was interpreted by Li et al. [2016] in the context of a buckling or instability model, whereby the sedimentary response to the collision between the Cocos Ridge and the Middle American Trench leads to the formation of such hiatuses.

4.3.2. The Pliocene and Lowermost Pleistocene

In our materials this period is characterized by a short interval that according to the age model, represents ~40 m of sediments. Due to the poor silica preservation in these samples (supporting information Table S1) and the scarcity of Pliocene materials, in agreement with geochemical shipboard analysis [Harris et al., 2013], our age assignments for this period are based on nannofossils datums and tephras; no radiolarians biozones could be established. A major drop characterizes the three Pliocene samples in species richness and diversity (Figure 7). The nodal analysis shows that the dominant radiolarians in these samples are *Spongotrochus* spp., *Phorticium pylonium* group, *Acrosphaera* spp., and *Stylosphaera* spp. At present, these species have rather

wide latitudinal ranges [Boltovskoy *et al.*, 2010], which complicates their use as paleoceanographic indicators. On the other hand, the abundance drop of *Spongurus* spp. (Figure 7 and supporting information Figure S5), could suggest a transition to warmer water conditions. During the Pliocene, the sites investigated were located north of the equator, and were influenced by the warmer water of the ECC. A tectonic translocation of the Cocos Plate into an area of lower nutrients and productivity probably occurred during this period. The Pliocene climate has been the subject of many studies, most of which agree that it was similar to present-day El Niño–Southern Oscillation (ENSO) conditions, characterized by warmer water in the Eastern Equatorial Pacific. This ENSO situation in the Pacific was probably permanent from ~4.5 to 3 Ma [Ravelo *et al.*, 2004]. Both tectonics and climate seem to have affected that area, causing drops in the preservation of biogenic silica during the Pliocene. Molina-Cruz [1977, 1997] reported extremely low radiolarian abundances during the late Pliocene in the Equatorial Pacific. He interpreted this in terms of high terrigenous inputs from the regional uplift, associated with the final stages of the CAS. Geochemical shipboard analyses [Harris *et al.*, 2013] show that enhanced terrigenous input started during the early Pliocene, quartz and plagioclase being the principal minerals. Kamikuri *et al.* [2009b] noticed a deepening of the thermocline, a weakening of upwelling, and the development of a warm pool in the eastern Equatorial Pacific during the interval from 9.8 to 4.2 Ma.

4.3.3. The Pleistocene

The Pleistocene corresponds to radiolarian zones RN13 to RN16 (Figure 10). The cluster/nodal analyses performed point at the dominance of ecologically significant radiolarians during this period, such as *Actinomma langii*, *Cycladophora davisiana*, and *Dictyophimus infabricatus* (Figure 7). The presence of these species suggests that cold waters played an important role in the formation of these deposits, and/or that the area was influenced by coastal upwelling (see Table 1). This result aligns with those of Kamikuri *et al.* [2009b], who reported that this area had been under the influence of upwelling since early Pliocene (4.2 Ma), as a result of the weakening of the East Pacific Warm Pool and the expansion of the oxygen minimum zone in the intermediate layer. In our study, colder conditions seem to start in the early Pleistocene (rather than in the Pliocene), which can be attributed to differences in the geographic locations of the materials investigated, and to the scarcity of Pliocene radiolarians in our samples.

5. Conclusions

The radiolarian record in sites U1381 and U1414 of the IODP Expedition 344 is variable, with large sections containing abundant and well-preserved biogenic remains, and others exhibiting low abundance and/or poor preservation.

An important hiatus of approximately 8 my is present in Hole U1381C in the interval of radiolarian zones RN6 to RN12, which are totally absent. The sequence of Hole U1414A is continuous, but presents a 100 m thick interval with scarce siliceous microfossils, missing the biozones RN9 to RN12. The ages of this zone were assigned based on nannofossil data and tephra ages.

On the basis of the radiolarian assemblages recovered, three paleoceanographic situations were recognized:

1. In the late Miocene, the area was dominated by cold-water currents, including the South Equatorial Current and the Peru Current and its associated upwelling water. *Spongurus* spp. dominated this cold-water environment.
2. The Pliocene and lowermost Pleistocene were characterized by poor silica preservation, possibly due to the displacement of the corresponding locality from a cold water, high nutrient area to a warm water, low nutrient zone (in the area of the Equatorial Countercurrent). The scarcity of siliceous remains is also probably due to the El Niño-like conditions that have been reported to characterize this period in the eastern equatorial Pacific, as well as to the high terrigenous continental input characterized by enhanced proportions of quartz and plagioclase.
3. In the Pleistocene, sediments were dominated by a tropical fauna, but with significant proportions of cold-water species, most probably associated with coastal upwelling water.

References

- Bacon, C., D. Silvestro, C. Jaramillo, B. Tilston Smith, P. Chakrabarty, and A. Antonelli (2015), Biological evidence supports an early and complex emergence of the Isthmus of Panama, *Proc. Natl. Acad. Sci., U. S. A.*, 112(19), 6110–6115.
- Barckhausen, U., C. R. Ranero, R. Von Huene, S. C. Cande, and H. A. Roeser (2001), Revised tectonic boundaries in the Cocos Plate off Costa Rica: Implications for the segmentation of the convergent margin and for plate tectonic models, *J. Geophys. Res.*, 106(B9), 19,207–19,220.

Acknowledgments

Supporting data are available on the internet site of the journal Geochemistry Geophysics Geosystems. The Swiss IODP committee is acknowledged for giving us the opportunity to participate in this project. Shipboard data and samples were provided by the Integrated Ocean Drilling Program (IODP). We thank the IODP Scientific Party for comments and discussions. We are grateful to Valeria Moldano (Biology Department, University of Lausanne) for her advice on statistical analyses. The Swiss National Science Foundation (SNSF) financially supported this research through projects 200021-134873 and 200020-143894. The comments of Noritoshi Suzuki and Kristina Pascher greatly helped to improve an earlier draft of this work.

- Baumgartner, P. O. (2013), Mesozoic radiolarites—Accumulation as a function of sea surface fertility on Tethyan margins and in ocean basins, *Sedimentology*, *60*(1), 292–318.
- Boesch, D. F. (1977), Application of numerical classification in ecological investigations of water pollution, *Ecol. Res. Ser., Spec. Sci. Rep. 77*, EPA-600/3-77-033, 115 pp., Natl. Tech. Inform. Serv., Corvallis, Oreg.
- Boltovskoy, D. (1987), Sedimentary record of Radiolarian biogeography in the Equatorial to Antarctic Western Pacific Ocean, *Micropaleontology*, *33*(3), 267–281.
- Boltovskoy, D. (1994), The sedimentary record of pelagic biogeography, *Prog. Oceanogr.*, *34*(2–3), 135–160.
- Boltovskoy, D., and W. R. Riedel (1987), Polycystine radiolaria of the California Current region: Seasonal and geographic patterns, *Mar. Micropaleontol.*, *12*(1), 65–104.
- Boltovskoy, D., and N. Correa (2016), Biogeography of Radiolaria Polycystina (Protista) in the World Ocean, *Prog. Oceanogr.*, *149*, 82–105.
- Boltovskoy, D., and N. Correa (2017), Planktonic equatorial diversity troughs: fact or artifact? Latitudinal diversity gradients in Radiolaria, *Ecology*, *98*, 112–124.
- Boltovskoy, D., V. A. Alder, and A. Abelmann (1993), Annual flux of radiolaria and other shelled plankters in the eastern equatorial Atlantic at 853 m: Seasonal variations and polycystine species-specific responses, *Deep Sea Res., Part I*, *40*(9), 1863–1895.
- Boltovskoy, D., E. Uliana, and G. Wefer (1996), Seasonal variation in the flux of microplankton and radiolarian assemblage compositions in the northeastern tropical Atlantic at 2,195 m, *Limnol. Oceanogr.*, *41*(4), 615–635.
- Boltovskoy, D., S. A. Kling, K. Takahashi, and K. Bjørklund (2010), World atlas of distribution of Recent Polycystina (Radiolaria), *Palaeontol. Electron.*, *13*(3), 230.
- Boyer, T. P., et al. (2013), World Ocean Database in NOAA Atlas NEIS 72, edited by S. Levitus and A. Mishonov, NOAA, Silver Spring, Md.
- Brierley, C. M., and A. V. Fedorov (2016), Comparing the impacts of Miocene-Pliocene changes in inter-ocean gateways on climate: Central American Seaway, Bering Strait, and Indonesia, *Earth Planetary Sci. Lett.*, *444*, 116–130.
- Coates, A., J. Jackson, L. Collins, T. Cronin, H. Dowsett, L. Bybell, P. Jung, and J. Obando (1992), Closure of the Isthmus of Panama: The near-shore marine record of Costa Rica and western Panama, *GSA*, *104*(7), 814–828.
- Coates, A. G., L. S. Collins, and M.-P. Aubry, and W. A. Berggren (2004), The Geology of the Darien, Panama, and the late Miocene-Pliocene collision of the Panama arc with northwestern South America, *Geol. Soc. Am. Bull.*, *116*, 1327–1344.
- De Wever, P., P. Dumitrica, J. P. Caulet, C. Nigrini, and M. Caridroit (2001), *Radiolarians in the Sedimentary Record*, 533 pp., Gordon and Breach Sci. Publ., Amsterdam.
- Farrell, J. W., I. Raffi, T. R. Janecek, T. W. Murray, M. Levitan, K. A. Dadey, K.-C. Emeis, M. Lyle, J. A. Flores, and S. Hovan (1995), Late Neogene sedimentation patterns in the Eastern Equatorial Pacific Ocean, in *Proceedings of the Ocean Drilling Program, Scientific Results*, vol. 138, edited by N. G. Pisias et al., pp. 717–756, Integr. Ocean Drill. Program, College Station, Tex.
- Fatela, F., and R. Taborda (2002), Confidence limits of species proportions in microfossil assemblages, *Mar. Micropaleontol.*, *45*(2), 169–174.
- Fedorov, A. V., P. S. Dekens, M. McCarthy, A. C. Ravelo, P. B. de Menocal, M. Barreiro, R. Pacanowski, and S. G. Philander (2006), The Pliocene Paradox (Mechanism for a Permanent El Niño), *Science*, *312*, 1485–1489.
- Gradstein, F. M., J. G. Ogg, M. Schmitz, and G. Ogg (2012), *The Geologic Time Scale*, Elsevier, Amsterdam.
- Goll, R. (1980), Pliocene-Pleistocene radiolarians from the East Pacific Rise and the Galapagos spreading center, *Deep Sea Drill. Proj. Leg 54. DP Rep.*, pp. 425–453, Initial Rep. Deep Sea Drilling Project, US Govern. Print. Off., Washington, D. C.
- Hammer, Ø., D. A. T. Harper, and P. D. Ryan (2001) PAST: Paleontological statistics software package for education and data analysis. *Palaeontol. Electron.*, *4*(1), 1–9.
- Harris, R. N., et al. (2013), Input Site U1414 and U1381, *Proc. Integr. Ocean Drill. Program*, *344*, 1–87.
- Haslett, S. K. (1992), Early Pleistocene glacial-interglacial radiolarian assemblages from the eastern equatorial Pacific, *J. Plankton Res.*, *14*, 1553–1563.
- Haslett, S. K. (1994), High-resolution radiolarian abundance data through the Late Pliocene Olduvai subchron of ODP Hole 677A (Panama Basin, eastern equatorial Pacific), *Rev. Esp. Micropaleontol.*, *26*, 127–162.
- Haslett, S. K. (1995), Mapping Holocene upwelling in the eastern equatorial Pacific using Radiolaria, *Holocene*, *5*(4), 470–478.
- Haug, G. H., R. Tiedemann, R. Zahn, and A. C. Ravelo (2001), Role of Panama uplift on oceanic freshwater balance, *Geology*, *29*(3), 207–210.
- Hollis, C. J., and H. L. Neil (2005), Sedimentary record of radiolarian biogeography, offshore eastern New Zealand, *N. Z. J. Mar. Freshwater Res.*, *39*(1), 165–192.
- Johnson, D. A., and C. A. Nigrini (1980), Radiolarian biogeography in surface sediments of the western Indian Ocean, *Mar. Micropaleontol.*, *5*(1), 111–152.
- Johnson, D. A., and C. A. Nigrini (1982), Radiolarian biogeography in surface sediments of the eastern Indian Ocean, *Mar. Micropaleontol.*, *7*(3), 237–281.
- Johnson, D. A., D. A. Schneider, C. A. Nigrini, J.-P. Caulet, and D. V. Kent (1989), Pliocene-Pleistocene radiolarian events and magnetostratigraphic calibrations for the tropical Indian Ocean, *Mar. Micropaleontol.*, *14*(1–3), 33–66.
- Jombart, T. (2008), ADEGENET: R package for the multivariate analysis of genetic markers, *Bioinformatics*, *24*, 1403–1405.
- Jombart, T., and C. Collins (2015), *A tutorial for Discriminant Analysis of Principal Components (DAPC) using adegenet 2.0.0*, Imp. Coll. London MRC Cent. for Outbreak Anal. and Modell., London, U. K.
- Jombart, T., D. Sébastien, and F. Balloux (2010), Discriminant analysis of principal components: A new method for the analysis of genetically structured populations, *BioMed Central Genet.*, *11*(94), 1–15.
- Kamikuri, S., I. Motoyama, H. Nishi, and M. Iwai (2009a), Neogene radiolarian biostratigraphy and faunal evolution rates in the eastern equatorial Pacific ODP Sites 845 and 1241, *Acta Palaeontol. Pol.*, *54*(4), 713–742.
- Kamikuri, S., I. Motoyama, H. Nishi, and M. Iwai (2009b), Evolution of Eastern Pacific Warm Pool and upwelling processes in the middle Miocene based on analysis of radiolarian assemblages: Response to Indonesian and Central American Seaways, *Palaeogeogr. Palaeoclimatol. Palaeoecol.*, *280*(3–4), 469–479.
- Keller, G., and J. A. Barron. (1983) Paleoclimatographic implications of Miocene deep-sea hiatus, *Geol. Soc. Am. Bull.*, *94*(5), 590–613.
- Kessler, W. S. (2006), The circulation of the eastern tropical Pacific: A review, *Prog. Oceanogr.*, *69*(2–4), 181–217.
- Kling, S. A. (1979), Vertical distribution of polycystine radiolarians in the central North Pacific, *Mar. Micropaleontol.*, *4*(1), 295–318.
- Kling, S. A., and D. Boltovskoy (1995), Radiolarian vertical distribution patterns across the Southern California current, *Deep Sea Res., Part I*, *42*(2), 191–231.
- Krapp, M., and J. H. Jungclaus (2011), The middle Miocene climate as modelled in an atmosphere-ocean-biosphere model, *Clim Past*, *7*, 1169–1188.
- Li, Y.-X., X. Zhao, L. Jovane, K. E. Petronotis, Z. Gong, and S. Xie (2015), Paleomagnetic constraints on the tectonic evolution of the Costa Rican subduction zone: New results from sedimentary successions of IODP drill sites from the Cocos Ridge, *Geochem. Geophys. Geosyst.*, *16*, 4479–4493, doi:10.1002/2015GC006058.

- Lyle, M., K. A. Dadey, and J. W. Farrell (1995), The late Miocene (11–8 Ma) eastern Pacific carbonate crash: Evidence for reorganization of deep-water circulation by the closure of the Panama Gateway, in *Proceedings of the Ocean Drill. Program, Sci. Results*, vol. 138, edited by N. G. Pisias et al., pp. 821–838, Ocean Drill. Program, College Station, Tex.
- Lyle, M., J. Barron, T. Bralower, W. Huber, A. O. Lyle, A. C. Ravelo, D. K. Rea, and P. Wilson (2008), Pacific Ocean and Cenozoic evolution of climate, *Rev. Geophys.*, 46, RG2002, doi:10.1029/2005RG000190.
- Martini, E., and T. Worsley (1970), Standard Neogene calcareous nannoplankton zonation, *Nature*, 225, 289–290.
- Meschede, M., and U. Barckhausen (2000), Late tectonic evolution of the Cocos-Nazca spreading center, in *Proceedings of the Ocean Drilling Program, Scientific Results*, vol. 170, edited by E. A. Silver, G. Kimura, and T. H. Shipley, pp. 1–10, Ocean Drill. Program, College Station, Tex.
- Mix, A. C., et al. (2003), Southeast Pacific Paleooceanographic Transects. Covering Leg 202 of the cruises of the Drilling Vessel *JOIDES Resolution* Valparaiso, Chile, to Balboa, Panama. Sites 1232–1242, in *Proceedings of the Ocean Drilling Program, Initial Reports*, vol. 202, edited by K. L. May, A. T. Miller, and L. L. Peters, Southeast Pac. Paleooceanogr. Transect, doi:10.2973/odp.proc.ir.202.2003.
- Molina-Cruz, A. (1977), Radiolarian assemblages and their relationship to the oceanography of the subtropical southeastern Pacific, *Mar. Micropaleontol.*, 2(1), 315–352.
- Molina-Cruz, A. (1997), Closing of the Central American Gateway and its effects on the distribution of Late Pliocene radiolarians in the eastern tropical Pacific, *Tectonophysics*, 281(1–2), 105–111.
- Molnar, P., and M. Cane (2002), El Niño's tropical climate and teleconnections as a blueprint for pre-Ice age climates, *Paleoceanography*, 17(2), 11-1–11-1.
- Montano, V., V. Marcari, M. Pavanello, O. Anyaele, D. Comas, G. Destro-Bisol, and C. Batini, (2013) The influence of habitats on female mobility in Central and Western Africa inferred from human mitochondrial variation, *BioMed Central Evol. Biol.*, 13(24), 2–19.
- Montes, C., A. Cardona, C. Jaramillo, A. Pardo, J. C. Silva, V. Valencia, C. Pérez-Ayala, L. C. Angel, L. A. Rodríguez-Parra, and H. Niño (2015), Middle Miocene closure of the Central American Seaway, *Science*, 348(6231), 226–228.
- Moore, J. T. C. (1995), Radiolarian stratigraphy, Leg 138, in *Proceedings of the Ocean Drilling Program, Scientific Results*, Eastern Equatorial Pacific Sites 844–854, vol. 138, edited by N. G. Pisias et al., pp. 191–232, Ocean Drill. Program, College, Tex.
- Moore, T. C. J., T. H. Van Andel, C. Sancetta, and N. G. Pisias (1978), Cenozoic hiatuses in pelagic sediments, *Micropaleontology*, 24(2), 113–138.
- Moore, T. C. J., L. H. Burckle, K. Geitzenauer, A. Molina-Cruz, J. H. Robertson, H. Sachs, C. Sancetta, J. Thiede, P. Thompson, and C. Wenkam (1980), The reconstruction of sea surface temperatures in the Pacific Ocean of 18,000 B.P., *Mar. Micropaleontol.*, 5(1), 215–247.
- Moore, T. C., N. J. Skackleton, and N. G. Pisias (1993), Paleooceanography and the diachrony of radiolarian events in the eastern equatorial Pacific, *Paleoceanography* 8(5), 567–586.
- Morley, J. J. (1977), Upper Pleistocene climatic variations in the South Atlantic derived from a quantitative radiolarian analysis: Accent on the last 18000 years, PhD thesis, 282 pp., Columbia Univ., New York.
- Nigrini, C. A. (1967), *Radiolaria in Pelagic Sediments From the Indian and Atlantic Oceans*, 125 pp., Univ. of California Press, Calif.
- Nigrini, C. A. (1968), Radiolaria from eastern tropical Pacific sediments, *Micropaleontology*, 51–63.
- Nigrini, C. A. (1977), Tropical Cenozoic Artostrobiidae (Radiolaria), *Micropaleontology*, 23(3), 241–269, *Micropaleontology*, 14(1), 51–63.
- Nigrini, C. A., and J.-P. Caulet (1992), Late Neogene radiolarian assemblages characteristic of Indo-Pacific areas of upwelling, *Micropaleontology*, 38(2), 139–164.
- Nigrini, C. A., and G. Lombardi (1984), A guide to Miocene Radiolaria. Cushman Foundation for Foraminiferal Research, *Spec. Publ.* 22, S1–N206.
- O'Dea, A., et al. (2016), Formation of the Isthmus of Panama, *Sci. Adv.*, 2(8), 1–11.
- Ogg, J. G., G. M. Ogg, and F. M. Gradstein (2016), *A Concise Geologic Time Scale 2016*, Elsevier, Amsterdam.
- Okazaki, Y., K. Takahashi, H. Yoshitani, T. Nakatsuka, M. Ikehara, and M. Wakatsushi (2003), Radiolarians under the seasonally sea-ice covered conditions in the Okhotsk Sea: Flux and their implications for paleoceanography, *Mar. Micropaleontol.*, 49(3), 195–230.
- Okazaki, Y., K. Takahashi, J. Onodera, and M. C. Honda (2005), Temporal and spatial flux changes of radiolarians in the northwestern Pacific Ocean during 1997–2000, *Deep Sea Res., Part II*, 52(16–18), 2240–2274.
- Okazaki, Y., K. Takahashi, and H. Asahi (2008), Temporal Fluxes of Radiolarians along the W-E Transect in the Central and Western Equatorial Pacific, 1999–2002, *Micropaleontology*, 54(1), 71–85.
- Pagani, M., K. Freeman, and M. A. Arthur (1999), Late Miocene atmospheric CO₂ concentrations and the expansion of C4 grasses, *Science*, 285, 876–878.
- Pennington, J. T., K. L. Mahoney, V. S. Kuwahara, D. D. Kolber, R. Calienes, and F. P. Chavez (2006), Primary production in the eastern tropical Pacific: A review, *Prog. Oceanogr.*, 69(2–4), 285–317.
- Petrushevskaya, M. G. (1971), On the natural system of polycystine Radiolaria (Class Sarcodina), in *Proceedings of the II Planktonic Conference, Planktonic Conference 2nd, Roma, Italy*, edited by A. Farinacci, pp. 981–992, Technoscienza, Rome.
- Pisias, N. G., D. Murray, and A. Roelofs (1986), Radiolarian and silicoflagellate response to oceanographic changes associated with the 1983 El Niño, *Nature*, 320(6059), 259–262.
- Pisias, N. G., A. Roelofs, and M. Weber (1997), Radiolarian-based transfer functions for estimating mean surface ocean temperatures and seasonal range, *Paleoceanography*, 12(3), 365–379.
- Ravelo, A. C., D. H. Andreasen, M. Lyle, A. O. Lyle, and M. W. Wara (2004), Regional climate shifts caused by gradual global cooling in the Pliocene epoch, *Nature*, 429(6989), 263–267.
- Ravelo, A. C., P. S. Dekens, M. Matthew (2006), Evidence of El Niño-like conditions during the Pliocene, *GSA Today*, 16(3), 411.
- Renz, G. W. (1976), *The Distribution and Ecology of Radiolaria in the Central Pacific: Plankton and Surface Sediments*, University of California Press, Berkeley, Calif., Bulletin of the Scripps Institution of Oceanography of the University of California, 22. La Jolla, California, 267 pp.
- Rickaby, R. E. M., and P. Halloran (2005), Cool La Niña during the warmth of the Pliocene?, *Science*, 307, 1948–1952.
- Riedel, W. R., and A. Sanfilippo (1970), Radiolaria, Leg 4, Deep Sea Drilling Project, in *Initial Reports of the Deep Sea Drilling Program*, vol. 4, edited by R. G. Bader et al., pp. 503–575.
- Riedel, W. R., and A. Sanfilippo (1978), Stratigraphy and evolution of tropical Cenozoic radiolarians, *Micropaleontology*, 24(1), 61–96.
- Romesburg, H. C. (1984), *Cluster Analysis for Esearchers*, 334 pp., Lulu Press, N. C.
- Romine, K. (1985), Radiolarian biogeography and paleoceanography of the North Pacific at 8 Ma, in *Geological Society of America Memoirs, The Miocene Ocean: Paleooceanography and Biogeography*, vol. 163, edited by J. P. Kennett, pp. 237–272, Geol. Soc. Amer.
- Ryan, W. B. F., et al. (2009), Global multi-resolution topography synthesis, *Geochem. Geophys. Geosyst.*, 10, Q03014, doi:10.1029/2008GC002332.
- Sachs, J. P., D. Sachse, R. H. Smittenberg, Z. Zhang, D. S. Battisti, and S. Golubic (2009), Southward movement of the Pacific intertropical convergence zone AD 1400–1850, *Nat. Geosci.*, 2, 519–525.

- Sanfilippo, A., and C. A. Nigrini (1998) Code numbers for Cenozoic low latitude radiolarian biostratigraphic zones and GPTS conversion tables, *Mar. Micropaleontol.*, 33(1–2), 121–117.
- Schindlbeck, J. C., S. Kutterolf, A. Freundt, S. M. Straub, K. L. Wang, M. Jegen, S. R. Hemming, A. T. Baxter, and M. I. Sandoval (2015), The Miocene Galapagos ash layer record of Integrated Ocean Drilling Program Legs 334 and 344: Ocean-island explosive volcanism during plume-ridge interaction, *Geology*, 43, 599–602.
- Schindlbeck, J. C., S. Kutterolf, A. Freundt, G. E. Alvarado, K. L. Wang, S. M. Straub, S. R. Hemming, M. Frische, and J. D. Woodhead (2016a), Late Cenozoic tephrostratigraphy offshore the southern Central American Volcanic Arc: 1. Tephra ages and provenance, *Geochem. Geophys. Geosyst.*, 17, 4641–4668, doi:10.1002/2016GC006503.
- Schindlbeck, J. C., S. Kutterolf, A. Freundt, S. M. Straub, P. Vannucchi, and G. E. Alvarado (2016b), Late Cenozoic tephrostratigraphy offshore the southern Central American Volcanic Arc: 2. Implications for magma production rates and subduction erosion, *Geochem. Geophys. Geosyst.*, 17, 4585–4604, doi:10.1002/2016GC006504.
- Shannon, C. E. (1948), A mathematical theory of communication, *Bell Syst. Tech. J.*, 27, 379–423, 623–656.
- Stavenhagen, A. U., R. H. FlüE, C. R. Ranero, K. D. McIntosh, T. H. Shipley, S. Augustin, G. Leandro, S. José, A. Schulze, and J. J. Dañobeitia (1997), Seismic wide-angle investigations in Costa Rica—A crustal velocity model from the Pacific to the Caribbean coast, *Z. Geol. Paläontol.*, 3(6), 393–408.
- Stewart, R. H. (2008), Equatorial processes, in *Introduction to Physical Oceanography*, pp. 235–254, Dep. of Oceanogr., Texas A&M Univ.
- Takahashi, K. (1991) Radiolaria: Flux, ecology, and taxonomy in the Pacific and Atlantic, *Ocean Biocoenosis Ser.*, vol. 3, 310 pp., Woods Hole Oceanogr. Inst., Mass.
- van Hinsbergen, D. J. J., L. V. de Groot, S. J. van Schaik, W. Spakman, P. K. Bijl, A. Sluijs, C. G. Langereis, and H. Brinkhuis (2015), A paleolatitude calculator for paleoclimate studies (model version 2.0), *PLoS One*, 10(6), e0126946.
- Watanabe, T., et al. (2011), Permanent El Niño during the Pliocene warm period not supported by coral evidence, *Nature*, 471, 209–211.
- Wara, M., A. C. Ravelo, and M. L. Delaney (2005), Permanent El Niño-Like conditions during the Pliocene warm period, *Science*, 309, 758–761.
- Welling, L. A. (1997), Environmental control of radiolarian abundance in the Central Equatorial Pacific and implications for paleoceanographic reconstructions, PhD thesis, 331 pp., Oregon State Univ., Oreg.
- Wyrtki, K. (1966), Oceanography of the eastern equatorial Pacific Ocean, *Oceanogr. Mar. Biol.*, 4(1), 33–68.
- Yu, Z., J. P. McCreary, W. S. Kessler, and K. Kelly (2000), Influence of Equatorial dynamics on the Pacific North Equatorial Countercurrent, *J. Phys. Oceanogr.*, 30(12), 3179–3190.
- Zachos, J., M. Pagani, L. Sloan, E. Thomas, and K. Billups (2001), Trends, rhythms, and aberrations in Global Climate 65 Ma to Present, *Science*, 292, 686–693.

[G cubed]

Supporting Information for

**Neogenepaleoceanography of the eastern equatorial Pacific based on the
radiolarian record of IODP drill sites off Costa Rica**

**María I. Sandoval¹†, Demetrio Boltovskoy², Alan T. Baxter^{3,4}, Peter O.
Baumgartner¹**

¹Institut des Sciences de la Terre, Université de Lausanne, Bâtiment Géopolis, CH 1015 Lausanne, Switzerland.

²Facultad de Ciencias Exactas y Naturales, Instituto de Ecología, Genética y Evolución de Buenos Aires (IEGEB), Universidad de Buenos Aires-CONICET, 1428 Buenos Aires, Argentina.

³School of Environmental and Rural Science, University of New England, Armidale, NSW 2351, Australia.

⁴Department of Earth and Planetary Sciences, McGill University, 3450 Rue University, Montreal, Canada.

Corresponding author: María Isabel Sandoval (mariaisabel.sandoval@ucr.ac.cr)

†Present address: Universidad de Costa Rica, Escuela Centroamericana de Geología, San Pedro de Montes de Oca, San José, Costa Rica

Contents of this file

Figures S1 to S5
Tables S1 to S4

Additional Supporting Information (Files uploaded separately)

Captions for Tables S1 to S4

Introduction

The following files are additional information regarding our research on IODP data, CRISP II. Enclosed you will find the radiolarians total abundances from the two holes (U1381C and U1414 A), radiolarians biozones assigned from the two holes, age model additional data and figures to better understand our study.

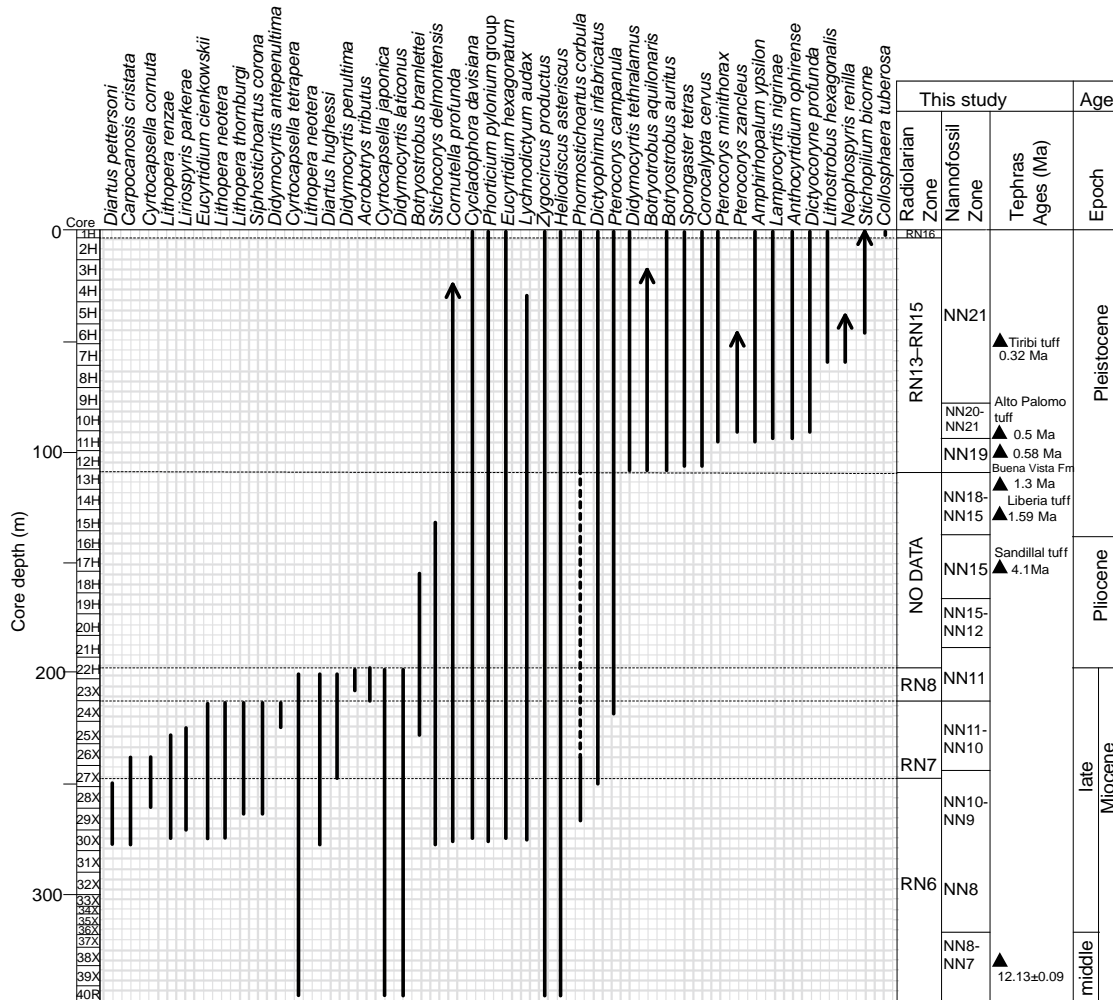


Figure S1. Diagram showing the distribution of common and biostratigraphically important radiolarians species in Hole U1414A. Calcareous nannofossil and tephra layer ages were used to correlate the radiolarian biozones. Solid lines with arrows: extant species. Dashed lines: species with known stratigraphic distribution but absent in our materials.

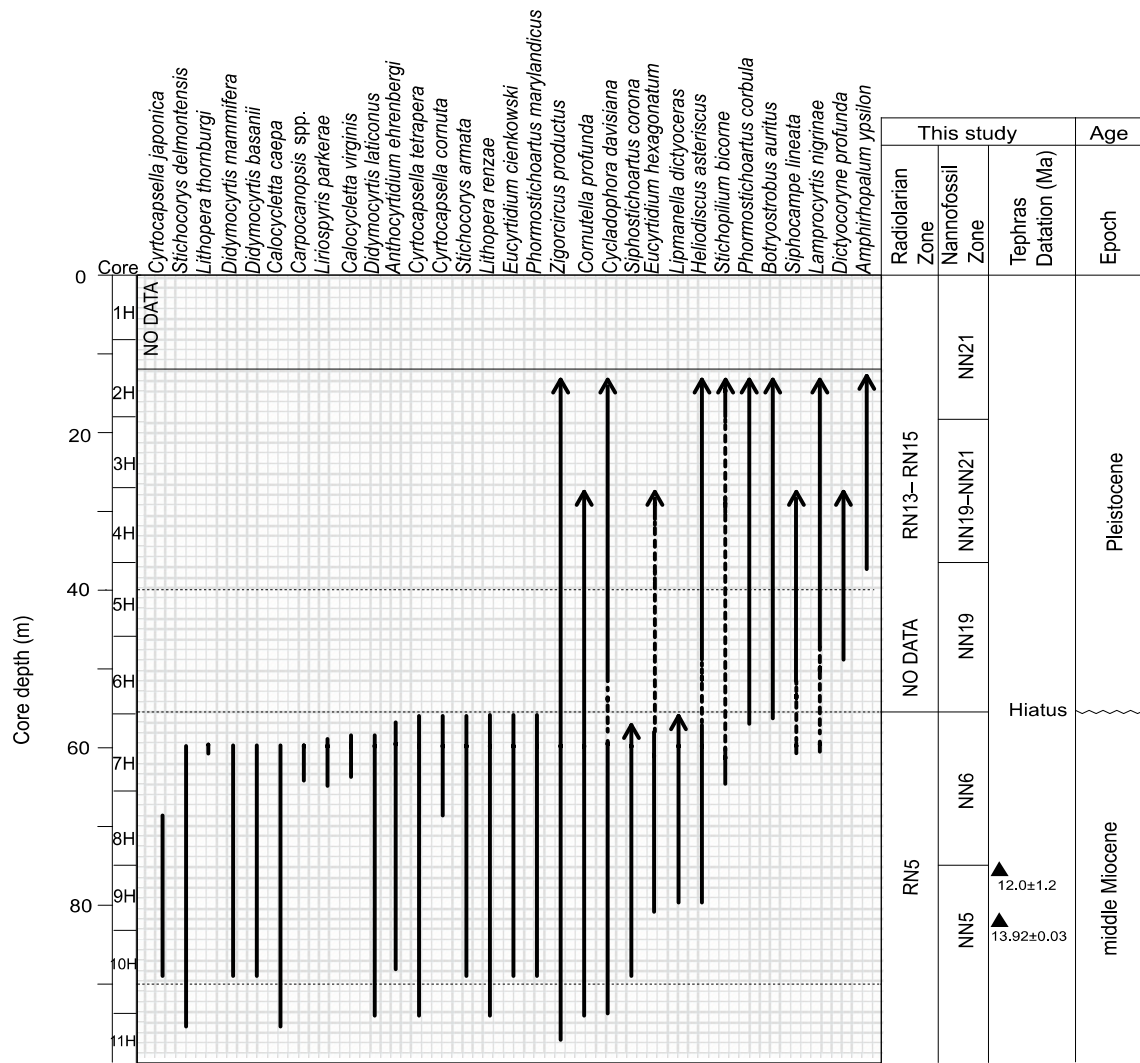


Figure S2. Diagram showing the distribution of common and biostratigraphically important radiolarians species in Hole U1381C. Calcareous nannofossil and tephra layer ages were used to correlate the radiolarian biozones. Solid lines with arrows: extant species. Dashed lines: species with known stratigraphic distribution but absent in our materials. The hiatus in this sequence is ~8 m.y. long.



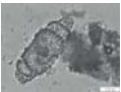


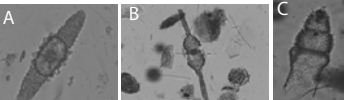
Radiolarian biozones	Standard tropical zonations and definitions	U1381C and U1414A observations	Age and correlation
RN16	<i>Collosphaera tuberosa</i> interval zone. Defined by the morphotypic first appearance of <i>Collosphaera tuberosa</i> coincident with the upper limit of the <i>Amphirhopalum ypsilon</i> zone (Nigrini and Sanfilippo, 2001).	U1381C: no data <i>Collosphaera tuberosa</i> (sample U1414A 1H-1W, 2–4 cm) U1414A: zone is The upper limit of <i>Amphirhopalum ypsilon</i> not well-marked. The sample is certainly at the base of RN16.	 Middle to Late Pleistocene Corresponds to NN21 nannoplankton zone.
RN15	<i>Stylatractus univertus</i> concurrent range zone. This zone was proposed by Johnson et al. (1989) to subdivide the RN16. It is located between the LO of <i>Stylatractus univertus</i> and the FO of <i>Collosphaera tuberosa</i> .	U1381C: no data U1414A: no data	Middle Pleistocene Corresponds to NN21 nannoplankton zone.
RN14	<i>Amphirhopalum ypsilon</i> interval zone. Corresponds to the stratigraphic interval between the FO of <i>Collosphaera tuberosa</i> and the LO of <i>Anthocytidium angulare</i> .	U1381C: no data <i>Amphirhopalum ypsilon</i> (sample U1414A 1H-1W, 24–26 cm) U1414A: Zone is not defined by radiolarians, only by nannofossils.	 Late-Early to Middle Pleistocene Corresponds to NN19 nannoplankton zone.
RN13	<i>Anthocytidium angulare</i> interval zone. Corresponds to the interval from the LO of <i>A. angulare</i> to the LO <i>Pterocanium prismatium</i> .	U1381C: no data U1414A: Biomarkers of the zone were not observed. The interval is tentatively assigned based on the FO of <i>Lithostrobos hexagonalis</i> and <i>Neophospyris renilla</i> , but these species are not good age indicators.	Late-Early to Middle Pleistocene Corresponds to NN19 nannoplankton zone.
RN8	<i>Didymocyrtis penultima</i> interval zone. Zone assigned by the evolutionary transition from <i>Stichocorys delmontensis</i> to <i>S. peregrina</i> and by the LO of <i>Diartus hughesi</i> .	U1381C: no data <i>Didymocyrtis penultima</i> (sample U1414A 22H-6W, 24–26 cm) U1414A: Zone assigned with the LO of <i>Diartus hughesi</i> and the evolutionary transition from <i>D. antepenultima</i> to <i>D. penultima</i> (from U1414A 24X-1W-24–26 to U1414A 25X-2W-24–26). Also includes the probable LO of <i>Cyrtocapsella tetrapera</i> , <i>Lithopera neotera</i> and <i>Didymocyrtis laticonus</i> ; but younger deposits are poor in radiolarians.	 Late Miocene Corresponds to NN11 nannoplankton zone.
RN7	<i>Didymocyrtis antepenultima</i> interval zone. Defined by the LO of <i>Diartus hughesi</i> and the evolutionary transition from <i>Diartus petterssoni</i> to <i>Diartus hughesi</i> .	U1381C: no data <i>Didymocyrtis antepenultima</i> (sample U1414A 23-1W-24–26 cm) U1414A: From U1414A 26X-7W-16–18 to U1414A 30X-8W-24–26.	 Late Miocene Corresponds to NN10 and NN11 nannoplankton zones.
RN6	<i>Diartus petterssoni</i> interval zone. Defined by the evolutionary transition from <i>Diartus petterssoni</i> to <i>Diartus hughesi</i> and the first occurrence of <i>Diartus petterssoni</i> .	U1381C: no data <i>Diartus petterssoni</i> (sample U1414A 31X-1W-24–26 cm) U1414A: From U1414A 26X-7W-16–18 to U1414A 30X-8W-24–26. The base of the zone is not clear, Age based from nannofossils.	 Early-Late Miocene Corresponds to NN7–NN10 nannoplankton zones.
RN5	<i>Dorcadospyris alata</i> interval zone. Defined by the FO of <i>Diartus petterssoni</i> and the evolutionary transition of <i>Dorcadospyris dentata</i> to <i>Dorcadospyris alata</i> .	U1381C: Biomarkers are not found. Zone based on the occurrence of A) <i>Didymocyrtis mammifera</i> B) <i>D. basanii</i> and C) <i>Stichocorys armata</i> (A, C sample U1381C 8H3W, 50–52 cm) (B sample U1381C 7H6W, 45–47 cm) U1414A: no data	 Late-Middle Miocene Corresponds to NN5 nannoplankton zone.

Figure S3. Assignment of the radiolarian biozones in Holes U1381C and U1414A in the context of the tropical radiolarian zonation proposed by Nigrini and Sanfilippo [2001].

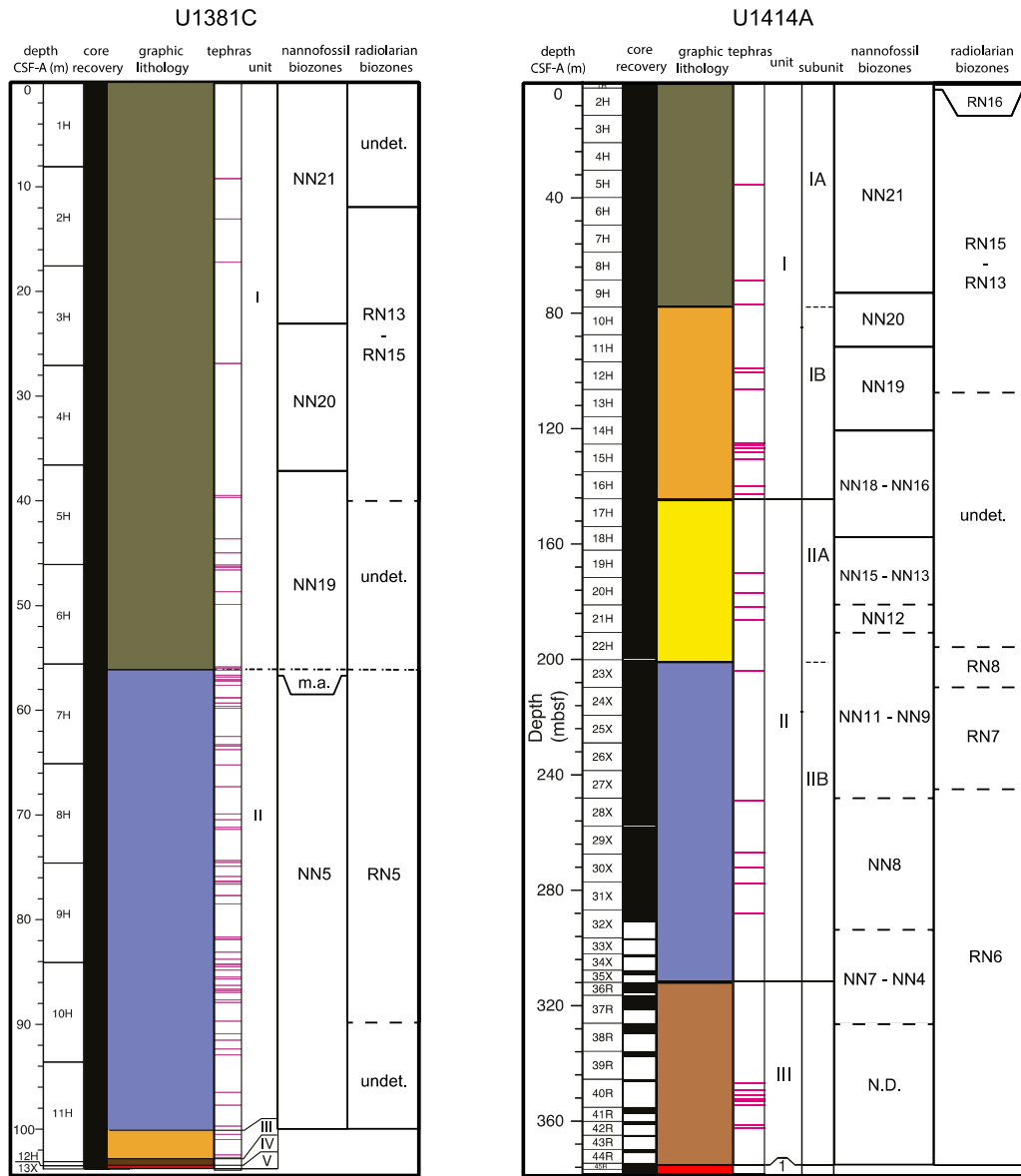


Figure. S4. Nannofossils and radiolarian biozones in Holes U1414A and U1381C.

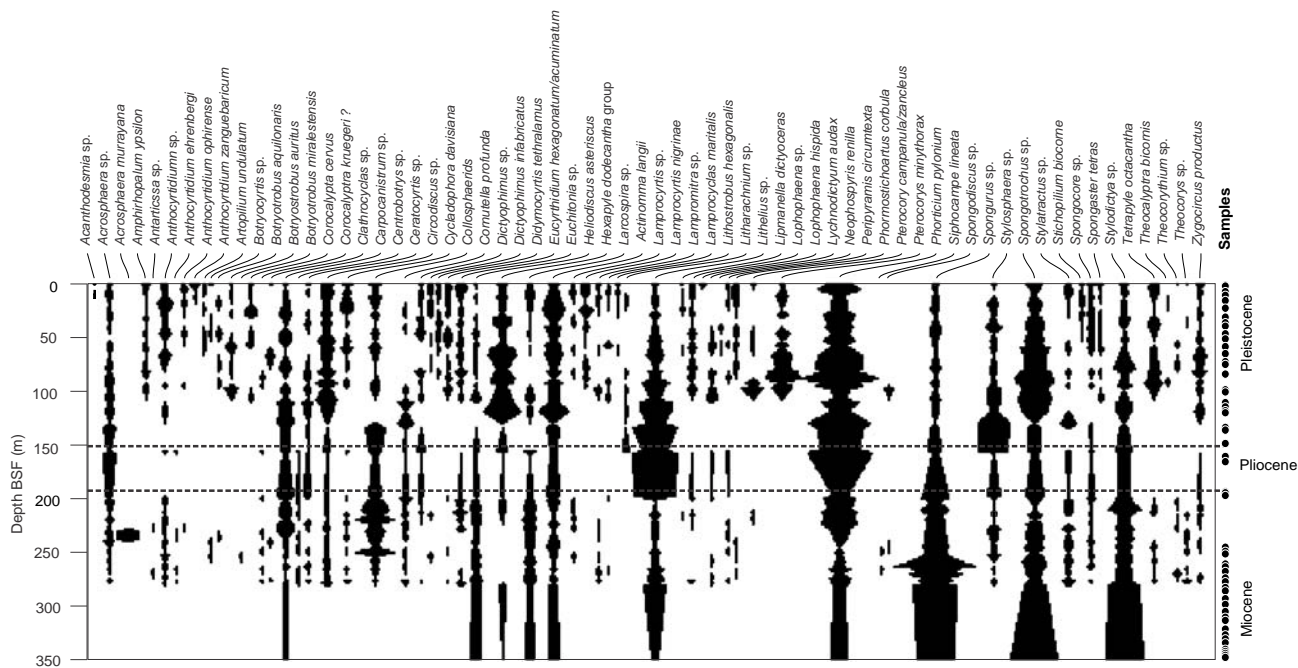


Figure. S5: Stratigraphic distribution of several radiolarian species and species group at Hole U1414A

Table S1. Radiolarian counts for Hole U1414A. Taxa used for paleoceanographic interpretations are denoted with asterisks.

Table S2. Radiolarian counts for Hole U1381A.

Table S3. Age markers for Hole U1381C. The depths for all age markers are midpoints calculated using the CSF-B scale.

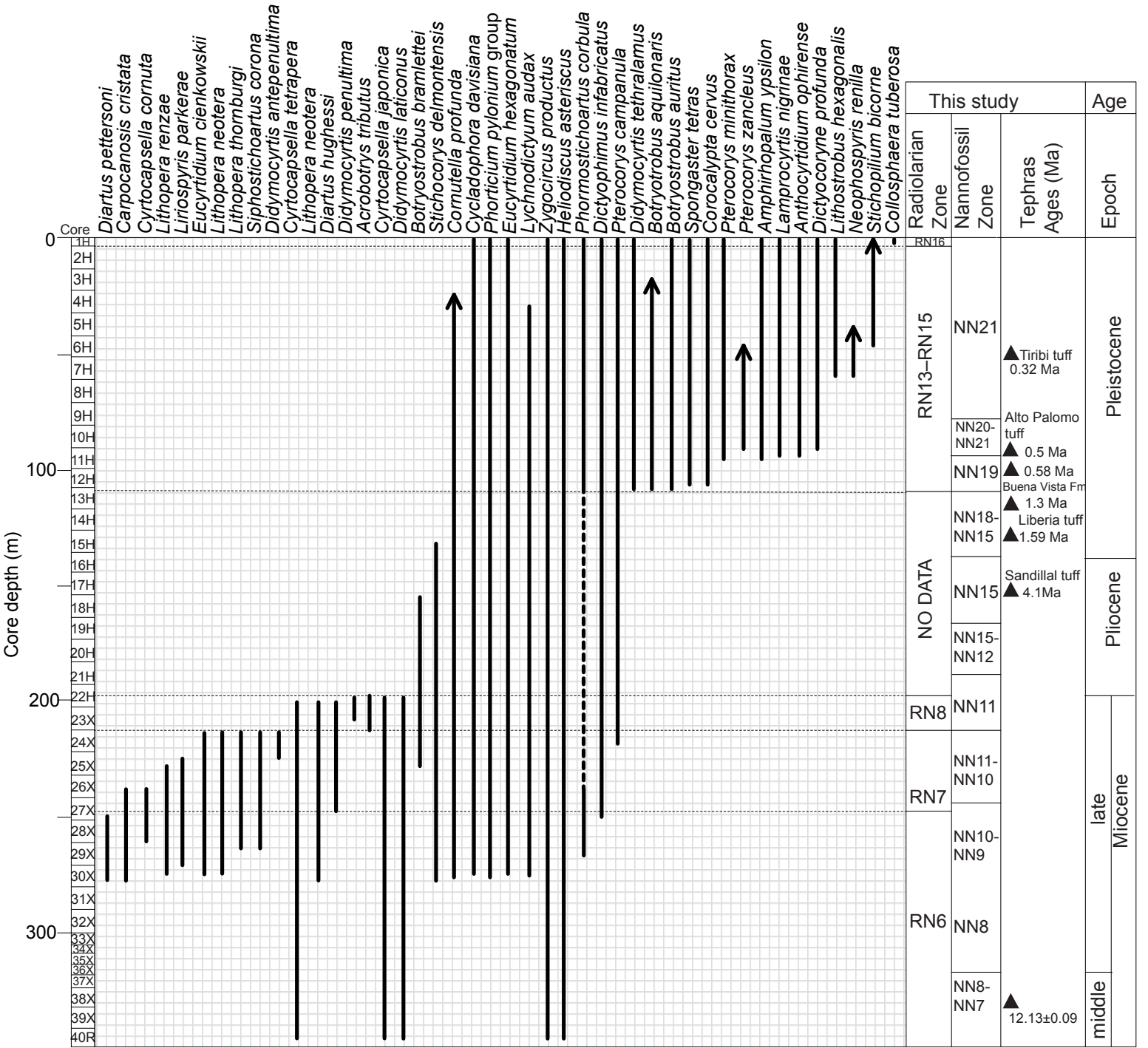
Table S4. Age markers for Hole U1414 A.

Table S3: Age markers for Site U1381C. The depths for all age markers are midpoints calculated using the CSF-B scale.

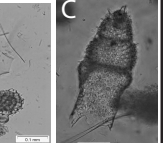
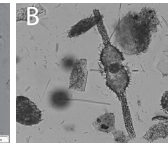
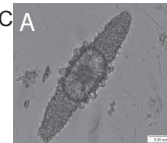
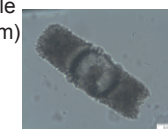
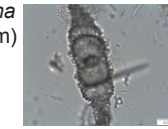
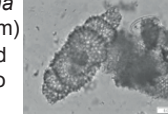
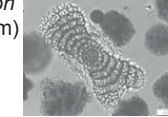
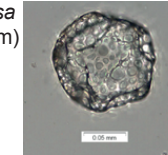
Type	Midpoint CSF-A (m)	Midpoint Error ± (m)	Top depth CSF-A (m)	Bottom depth CSF-A (m)	Age [Ma]	Error (Ma)	Nannofossil biomarkers	Sample Numbers	Reference	Depth Scale
Tephra correlation	6.16	0.01	6.15	6.17	0.0407			344-U1381C-1H-5, 15–17 cm	Schindlbeck et al., (2016a)	Midpoint CSF-A (m)
Tephra correlation	9.08	0.01	9.07	9.09	0.06			344-U1381C-2H-1, 97–99 cm	Schindlbeck et al., (2016a)	Midpoint CSF-A (m)
Nannofossils	22.86	4.80	18.06	27.66	0.290		FO <i>Emiliana huxleyi</i>		Harris et al., (2013)	Midpoint CSF-A (m)
Tephra correlation	26.765	0.025	26.74	26.79	0.322			344-U1381C-3H-7, 14–19 cm	Schindlbeck et al., (2016a)	Midpoint CSF-A (m)
Tephra correlation	39.41	0.01	39.4	39.42	0.5004			344-U1381C-5H-2, 130–132 cm	Schindlbeck et al., (2016a)	Midpoint CSF-A (m)
Tephra correlation	44.855	0.015	44.84	44.87	0.6248			344-U1381C-5H-6, 72–75 cm	Schindlbeck et al., (2016a)	Midpoint CSF-A (m)
Tephra correlation	46.035	0.005	46.03	46.04	0.6517			344-U1381C-5H-7, 41–42 cm	Schindlbeck et al., (2016a)	Midpoint CSF-A (m)
Tephra correlation	46.215	0.005	46.21	46.22	0.6648			344-U1381C-5H-7, 59–60 cm	Schindlbeck et al., (2016a)	Midpoint CSF-A (m)
Tephra correlation	46.285	0.005	46.28	46.29	0.671			344-U1381C-5H-7, 66–67 cm	Schindlbeck et al., (2016a)	Midpoint CSF-A (m)
Tephra correlation	46.56	0.01	46.55	46.57	0.6928			344-U1381C-5H-CC, 26–28 cm	Schindlbeck et al., (2016a)	Midpoint CSF-A (m)
Tephra correlation	48.57	0.01	48.56	48.58	0.8903			344-U1381C-6H-2, 93–95 cm	Schindlbeck et al., (2016a)	Midpoint CSF-A (m)
Tephra correlation	48.65	0.01	48.64	48.66	0.8973			344-U1381C-6H-2, 101–103 cm	Schindlbeck et al., (2016a)	Midpoint CSF-A (m)
Nannofossils	50.95	4.38	46.57	55.32	0.440		LO <i>Pseudoemiliana lacunosa</i>		Harris et al., (2013)	Midpoint CSF-A (m)
Tephra correlation	52.9	0.01	52.89	52.91	1.3134			344-U1381C-6H-5, 73–75 cm	Schindlbeck et al., (2016a)	Midpoint CSF-A (m)
Tephra correlation	52.95	0.01	52.94	52.96	1.3183			344-U1381C-6H-5, 78–80 cm	Schindlbeck et al., (2016a)	Midpoint CSF-A (m)
Tephra correlation	55.77	0.01	55.76	55.78	1.5945			344-U1381C-6H-7, 60–62 cm	Schindlbeck et al., (2016a)	Midpoint CSF-A (m)
Tephra correlation	55.81	0.01	55.8	55.82	1.5984			344-U1381C-6H-CC, 0–2 cm	Schindlbeck et al., (2016a)	Midpoint CSF-A (m)
Tephra	76.52	0.01	76.51	76.53	12	± 1.2		344-U1381C-9H-2, 41–43 cm	Schindlbeck et al., (2015)	Midpoint CSF-A (m)
Tephra	86.57	0.01	86.56	86.58	13.92	± 0.03		344-U1381C-10H-2, 96–98 cm	Schindlbeck et al., (2015)	Midpoint CSF-A (m)

Table S4: Age markers for Site U1414A.

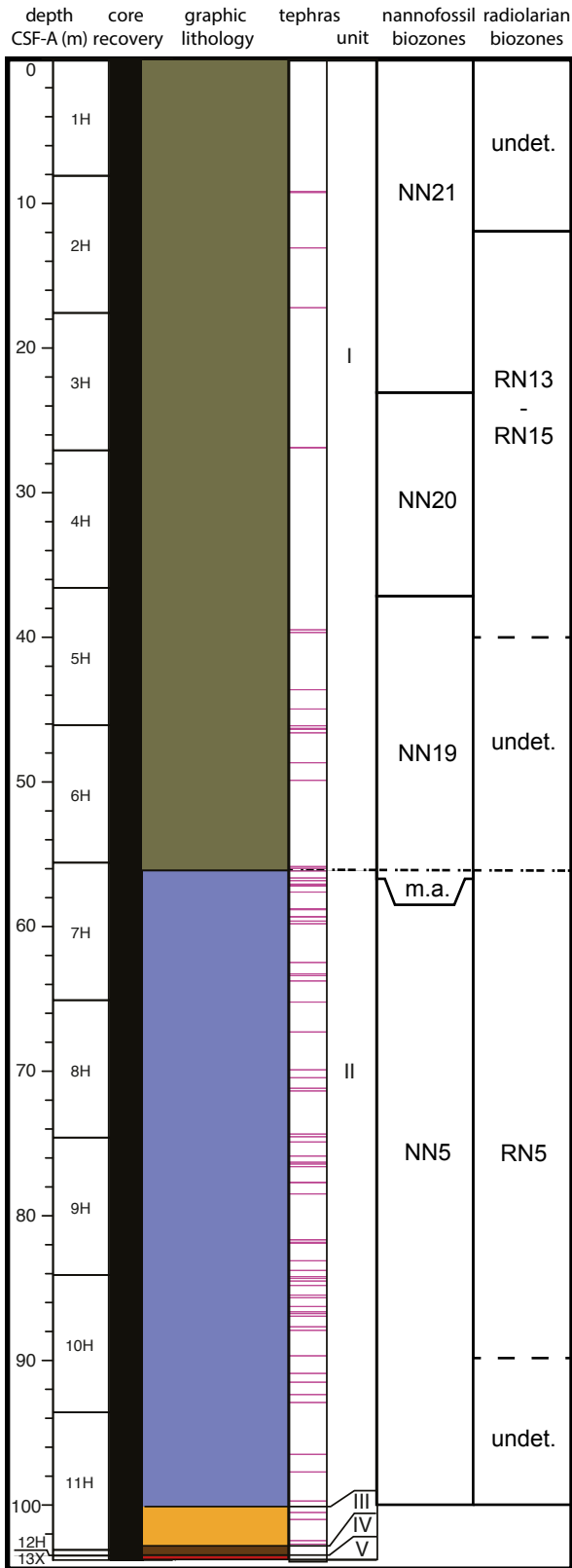
Marker Type	Midpoint CSF-A (m)	Midpoint Error ± (m)	Top depth CSF-A (m)	Bottom depth CSF-A (m)	Age [Ma]	Error (Ma)	Biomarkers	Sample Number	Reference	Depth scale
Tephra correlation	64.390	0.010	64.380	64.400	0.322			344-U1414A-8H-4, 98–100 cm	Schindlbeck et al., (2016a)	Midpoint CSF-A (m)
Tephra correlation	64.490	0.040	64.450	64.530	0.322			344-U1414A-8H-4, 105–113 cm	Schindlbeck et al., (2016a)	Midpoint CSF-A (m)
Tephra correlation	64.570	0.010	64.560	64.580	0.322			344-U1414A-8H-5, 3–5 cm	Schindlbeck et al., (2016a)	Midpoint CSF-A (m)
Tephra correlation	64.940	0.010	64.930	64.950	0.322			344-U1414A-8H-5, 40–42 cm	Schindlbeck et al., (2016a)	Midpoint CSF-A (m)
Tephra correlation	64.990	0.010	64.980	65.000	0.322			344-U1414A-8H-5, 45–47 cm	Schindlbeck et al., (2016a)	Midpoint CSF-A (m)
Tephra correlation	72.800	0.010	72.790	72.810	0.401			344-U1414A-9H-3, 139–141 cm	Schindlbeck et al., (2016a)	Midpoint CSF-A (m)
Nannofossils	73.490	4.810	68.680	78.300	0.290		FO <i>E. huxleyi</i>		Harris et al., (2013)	Midpoint CSF-A (m)
Tephra correlation	89.610	0.010	89.600	89.620	0.570			344-U1414A-11H-2, 70–72 cm	Schindlbeck et al., (2016a)	Midpoint CSF-A (m)
Tephra correlation	90.660	0.010	90.650	90.670	0.580			344-U1414A-11H-3, 25–27 cm	Schindlbeck et al., (2016a)	Midpoint CSF-A (m)
Nannofossils	92.430	4.720	87.710	97.150	0.440		LO <i>P. lacunosa</i>		Harris et al., (2013)	Midpoint CSF-A (m)
Tephra correlation	112.625	0.015	112.610	112.640	1.180			344-U1414A-13H-5, 21–24 cm	Schindlbeck et al., (2016a)	Midpoint CSF-A (m)
Tephra correlation	113.325	0.005	113.320	113.330	1.268			344-U1414A-13H-5, 92–93 cm	Schindlbeck et al., (2016a)	Midpoint CSF-A (m)
Tephra correlation	113.760	0.010	113.750	113.770	1.253			344-U1414A-13H-5, 135–137 cm	Schindlbeck et al., (2016a)	Midpoint CSF-A (m)
Tephra correlation	114.600	0.010	114.590	114.610	1.308			344-U1414A-13H-6, 69–71 cm	Schindlbeck et al., (2016a)	Midpoint CSF-A (m)
Tephra correlation	114.710	0.020	114.690	114.730	1.315			344-U1414A-13H-6, 79–83 cm	Schindlbeck et al., (2016a)	Midpoint CSF-A (m)
Tephra correlation	119.030	0.010	119.020	119.040	1.595			344-U1414A-14H-3, 12–14 cm	Schindlbeck et al., (2016a)	Midpoint CSF-A (m)
Nannofossils	120.875	4.925	115.950	125.800	2.060		LO <i>D. brouweri</i>		Harris et al., (2013)	Midpoint CSF-A (m)
Tephra correlation	129.620	0.010	129.610	129.630	2.060			344-U1414A-15H-3, 121–123 cm	Schindlbeck et al., (2016a)	Midpoint CSF-A (m)
Tephra correlation	129.960	0.010	129.950	129.970	2.084			344-U1414A-15H-4, 5–7 cm	Schindlbeck et al., (2016a)	Midpoint CSF-A (m)
Tephra correlation	133.670	0.010	133.660	133.680	2.339			344-U1414A-15H-6, 76–78 cm	Schindlbeck et al., (2016a)	Midpoint CSF-A (m)
Tephra correlation	151.670	0.030	151.640	151.700	3.350			344-U1414A-17H-5, 124–130 cm	Schindlbeck et al., (2016a)	Midpoint CSF-A (m)
Nannofossils	158.040	4.090	153.950	162.130	3.790		LO <i>R. pseudoumbilicus</i>		Harris et al., (2013)	Midpoint CSF-A (m)
Tephra correlation	159.090	0.020	159.070	159.110	4.150			344-U1414A-18H-5, 104–108 cm	Schindlbeck et al., (2016a)	Midpoint CSF-A (m)
Radiolarians	199.340	1.000	198.340	200.340	8.390		LO <i>Diartus hughesi</i>		this study	Midpoint CSF-A (m)
Radiolarians	208.890	1.050	207.840	209.940	8.390		FO <i>Didymocyrtis penultima</i>		this study	Midpoint CSF-A (m)
Radiolarians	248.650	1.190	247.460	249.840	8.840		FO <i>Diartus hughesi</i>		this study	Midpoint CSF-A (m)
Tephra	326.870	0.010	326.860	326.880	12.050	± 0.11		344-U1414A-38R-1, 76-78 cm	Schindlbeck et al., (2016a)	Midpoint CSF-A (m)



Radiolarian biozones	Standard tropical zonations and definitions	U1381C and U1414A observations	Age and correlation
RN16	<i>Collosphaera tuberosa</i> interval zone. Defined by the morphotypic first appearance of <i>Collosphaera tuberosa</i> coincident with the upper limit of the <i>Amphirhopalum ypsilon</i> zone (Nigrini and Sanfilippo, 2001).	U1381C: no data <i>Collosphaera tuberosa</i> (sample U1414A 1H-1W, 2–4 cm) U1414A: zone is The upper limit of <i>Amphirhopalum ypsilon</i> not well-marked. The sample is certainly at the base of RN16.	Middle to Late Pleistocene Corresponds to NN21 nannoplankton zone.
RN15	<i>Stylatractus universus</i> concurrent range zone. This zone was proposed by Johnson et al. (1989) to subdivide the RN16. It is located between the LO of <i>Stylatractus universus</i> and the FO of <i>Collosphaera tuberosa</i> .	U1381C: no data U1414A: no data	Middle Pleistocene Corresponds to NN21 nannoplankton zone.
RN14	<i>Amphirhopalum ypsilon</i> interval zone. Corresponds to the stratigraphic interval between the FO of <i>Collosphaera tuberosa</i> and the LO of <i>Anthocyrtidium angulare</i> .	U1381C: no data <i>Amphirhopalum ypsilon</i> (sample U1414A 1H-1W, 24–26 cm) U1414A: Zone is not define by radiolarians, only by nannofossils.	Late-Early to Middle Pleistocene Corresponds to NN19 nannoplankton zone.
RN13	<i>Anthocyrtidium angulare</i> interval zone. Corresponds to the interval from the LO of <i>A. angulare</i> to the LO <i>Pterocanium prismatium</i> .	U1381C: no data U1414A: Biomarkers of the zone were not observed. The interval is tentatively assigned based on the FO of <i>Lithostrobos hexagonalis</i> and <i>Neophospyris renilla</i> , but these species are not good age indicators.	Late-Early to Middle Pleistocene Corresponds to NN19 nannoplankton zone.
RN8	<i>Didymocyrtis penultima</i> interval zone. Zone assigned by the evolutionary transition from <i>Stichocorys delmontensis</i> to <i>S. peregrina</i> and by the LO of <i>Diartus hughesi</i> .	U1381C: no data <i>Didymocyrtis penultima</i> (sample U1414A 22H-6W, 24–26 cm) U1414A: Zone assigned with the LO of <i>Diartus hughesi</i> and the evolutionary transition from <i>D. antepenultima</i> to <i>D. penultima</i> (from U1414A 24X-1W-24–26 to U1414A 25X-2W-24–26). Also includes the probable LO of <i>Cyrtocapsella tetrapera</i> , <i>Lithopera neotera</i> and <i>Didymocyrtis laticonus</i> ; but younger deposits are poor in radiolarians.	Late Miocene Corresponds to NN11 nannoplankton zone.
RN7	<i>Didymocyrtis antepenultima</i> interval zone. Defined by the LO of <i>Diartus hughesi</i> and the evolutionary transition from <i>Diartus petterssoni</i> to <i>Diartus hughesi</i> .	U1381C: no data <i>Didymocyrtis antepenultima</i> (sample U1414A 23-1W-24–26 cm) U1414A: From U1414A 26X-7W-16–18 to U1414A 30X-8W-24–26.	Late Miocene Corresponds to NN10 and NN11 nannoplankton zones.
RN6	<i>Diartus petterssoni</i> interval zone. Defined by the evolutionary transition from <i>Diartus petterssoni</i> to <i>Diartus hughesi</i> and the first occurrence of <i>Diartus petterssoni</i> .	U1381C: no data <i>Diartus petterssoni</i> (sample U1414A 31X-1W-24–26 cm) U1414A: From U1414A 26X-7W-16–18 to U1414A 30X-8W-24–26. The base of the zone is not clear, Age based from nannofossils.	Early-Late Miocene Corresponds to NN7–NN10 nannoplankton zones.
RN5	<i>Dorcadospyrus alata</i> interval zone. Defined by the FO of <i>Diartus petterssoni</i> and the evolutionary transition of <i>Dorcadospyrus dentata</i> to <i>Dorcadospyrus alata</i> .	U1381C: Biomarkers are not found. Zone based on the occurrence of A) <i>Didymocyrtis mammifera</i> B) <i>D. basanii</i> and C) <i>Stichocorys armata</i> (A, C sample U1381C 8H3W, 50-52 cm) (B sample U1381C 7H6W, 45-47 cm) U1414A: no data	Late-Middle Miocene Corresponds to NN5 nannoplankton zone.



U1381C



U1414A

